Published in final edited form as:
Chem Commun (Camb). 2013 October 28; 49(84): 9704–9721. doi:10.1039/c3cc44268c.

Environmentally responsive MRI contrast agents

Gemma-Louise Davies, **Iris Kramberger**, and **Jason J. Davis***
Department of Chemistry, University of Oxford, South Parks Road, Oxford, OX1 3QZ, UK

Abstract

Biomedical imaging techniques can provide a vast amount of anatomical information, enabling diagnosis and the monitoring of disease and treatment profile. MRI uniquely offers convenient, non-invasive, high resolution tomographic imaging. A considerable amount of effort has been invested, across several decades, in the design of non toxic paramagnetic contrast agents capable of enhancing positive MRI signal contrast. Recently, focus has shifted towards the development of agents capable of specifically reporting on their local biochemical environment, where a switch in image contrast is triggered by a specific stimulus/biochemical variable. Such an ability would not only strengthen diagnosis but also provide unique disease-specific biochemical insight. This feature article focuses on recent progress in the development of MRI contrast switching with molecular, macromolecular and nanoparticle-based agents.

1. Introduction

There exist a wide variety of spatially resolved clinical imaging modalities, including positron emission tomography (PET), computed tomography (CT), ultrasound, optical imaging and magnetic resonance imaging (MRI).[1] Of these, MRI stands out through its combination of convenient non-invasive application, high spatial resolution, and tomographic capability. This modality can provide images of the anatomy and physiology of living subjects by rapidly mapping out the spatial distribution of the proton (^{1}H) signal intensity. Originally termed nuclear magnetic resonance imaging upon its discovery in the 1940s (renamed MRI in the 1970s due to deemed negative connotations associated with the term ‘nuclear’), this imaging technique works by exploiting the phenomenon of nuclear magnetic resonance (NMR) and, specifically, the reaction to a strong external magnetic field (B_0) of magnetic atomic nuclei, which absorb and re-emit electromagnetic waves at a characteristic radio frequency (RF). In a static magnetic field, nuclei process at a (Larmor) frequency (ω_0), which is linearly dependent on B_0 and the gyromagnetic ratio of the nucleus γ, according to eqn (1).

$$\omega_0 = \gamma \quad B_0 \quad (1)$$

The application of a RF pulse causes the net magnetisation vector associated with these processing and thermally equilibrated nuclei to flip from a position parallel to the external

*jason.davis@chem.ox.ac.uk; Fax: +44 (0)1865 272 690; Tel: +44 (0)1865 275 914 .

Europe PMC Funders Author Manuscripts

field to one transverse. The process of their relaxation back to the equilibrium state can occur by two different mechanisms, namely those which are longitudinal (or spin–lattice, T_1) or transverse (or spin–spin, T_2) in nature. An MR imaging system exploits the current generated by the motion of these relaxing magnetic moments by constructing a time domain NMR signal and using a Fourier transform to generate a frequency domain spectrum from which relaxation times may be derived. Images can be generated from these signals in different ways, most commonly by monitoring nuclear relaxation after a series of spaced RF pulses, which can then be spatially resolved electronically. Subsequently acquired image contrast in anatomical models is generated, in the first instance, from variance in water content across different body tissues. The inherently low sensitivity of MRI (arising primarily from the small energetic differential associated with nuclear Zeeman splitting) generally requires that this contrast be boosted through the use of added contrast agents, if it is to be diagnostically useful. Contrast agents work to enhance MR contrast by locally reducing T_1 and T_2 relaxation times.[2-5] Those that predominantly reduce T_1 are referred to as “positive” contrast agents and result in increases in signal intensity (bright contrast), whereas those which primarily affect T_2 are commonly known as “negative”, providing reductions in signal intensity (dark contrast). Clinically, T_1 agents offer higher spatial resolution and are not associated with false signal reading due to the existence of other signal draining sources in tissues that can plague T_2 modalities. The most common T_1 contrast agents currently used are paramagnetic gadolinium ion complexes (Gd^{3+}), due to their seven unpaired electrons, large magnetic moment and long electronic relaxation time (9–10 s), which contribute to enhanced relaxation according to the parameters set out in the Solomon, Bloembergen and Morgan (SBM) theory (*vide infra*).[6,7] Free Gd^{3+}, however, is toxic, disrupting physiological Ca^{2+} signalling;[8,9] kinetically robust chelation of Gd^{3+} with ligands such as tetraazacyclododecane-tetraacetic acid (DOTA) is, thus, commonly employed.[10,11] Such agents make up the majority of those in current clinical use, including gadopentetate dimeglumine (Magnevist), gadoterate meglumine (Dotarem), gadoteridol (ProHance) and gadodiamide (Omniscan).[12,13] This article will focus on progress made in further engineering such Gd binding scaffolds so as to engender high image contrast with additional responsiveness to chemical or biological stimuli of physiological relevance.

2. Molecular contrast agents (CAs)

In order to enhance image contrast obtained from molecular T_1 agents (such as those listed above), optimisation of the parameters that govern relaxivity have been investigated in detail for several decades, most commonly with concurrent reference to the SBM theory.[3,14,15] Indeed, relaxivity (r_1), defined by eqn (2), describing the change in relaxation rate ($\Delta(1/T_1) = \Delta R_1$) of water protons in the presence of a specified concentration of contrast agent ([CA]), is dependent on external field, temperature, the electronic properties of the paramagnetic centre, water residence time (τ_m), rotational correlation time (τ_R), first and second coordination sphere hydration (q), and the ion to water proton distance.[3] In general, enhanced relaxivity can be achieved by increasing the q value, shortening τ_m and increasing τ_R.

$$r_1 = \frac{\Delta\,(1/T_1)}{[\mathrm{CA}]} \quad (2)$$

T_1 relaxation originates, in part, from dipolar interactions between the imaged water protons and local paramagnetic species. The former may be inner-sphere (IS, those directly coordinated to the Gd^{3+} centre), second-sphere (SS, those hydrating the complex) or outer-sphere (OS, those diffusing near the chelate, governed by translational diffusion, τ_D), as depicted in Fig. 1, with their relaxation rates contributing to the overall relaxation rate according to eqn (3).

Inner-sphere contributions are thought to be the most important in the relaxation of molecular paramagnetic species (eqn (4), where T_{1m} is the longitudinal water proton relaxation time)[16] and have hence dominated investigations where chelating ligand structure has been tuned to facilitate relaxation enhancement,[3,6] or, more recently, report on immediate microenvironment.[3,17,18]

$$R_1 = R_1^{\mathrm{OS}} + R_1^{\mathrm{IS}} + R_1^{\mathrm{SS}} \quad (3)$$

$$R_1^{\mathrm{IS}} = \frac{[\mathrm{CA}]_q}{55.6}\left(\frac{1}{T_{1\mathrm{m}} + \tau_{\mathrm{m}}}\right) \quad (4)$$

2.1 Responsive molecular contrast agents

In living organisms, variations in tissue and cellular microenvironment can provide vital information about the status of healthy or diseased tissues, organs and tumours. A specific sensitivity of MR image contrast to a physiological or biochemical reaction in tissue is the main focus of the emerging discipline of functional MRI.[19] The most well-known example of this is blood-oxygen-level-dependent (BOLD) contrast, which depicts differences in blood oxygenation related to neural activity.[20] This technique provides MR contrast change through the imaging of haemoglobin (Hb) and the extreme sensitivity of this to oxygenation (an accompanying transformation of Hb from paramagnetic to diamagnetic).

The most common method of facilitating an MRI contrast response to environment with lanthanide macrocycles is through variations in hydration state (q value), often facilitated by conformation change.[16,21] The second-sphere water molecule dynamics of a chelate can also be manipulated by an environmental trigger, providing variation in MRI signal contrast.[22-25] Responsive conformation changes can alternatively result in a change in contrast agent molecular volume, affecting τ_R and hence T_{1m}.[26] Increases in the molecular weight of a contrast agent, through cross-linking or polymerisation, can also be prompted by an environmental stimulus, resulting in image contrast enhancement through the reduction of molecular tumbling rates (increasing τ_R). It is worth noting here that, in the design of agents for conventional MRI, permanent enhancement of signal contrast is the desired goal; in functional MRI, specific change in response to a physiological trigger (and the degree and specificity of relaxivity change) is more important than the absolute magnitude.

2.2 Bio-responsive molecular contrast agents

Potentially the most important developing class of responsive MRI is that based on agents that are acted on by pathologically relevant enzymes such as those associated with disease states including stroke, cerebral ischemia, cardiovascular or neurodegenerative inflammatory processes.[27] Pioneering work by Meade and co-workers in the late 1990s, for example, paved the way towards the development of responsive or 'smart' MRI contrast agents specifically designed to respond to an enzymatic cleavage.[28] Their work describes a family of 4,7,10-tri(acetic acid)-1-(2-β-galactopyranosylethoxy)-1,4,7,10-tetraazacyclo-dodecane gadolinium (EGad) contrast agents, whose galactopyranose groups are removed by β-galactosidase (an important reporter marker for monitoring gene expression), resulting in an irreversible transition from a weak to a strong relaxivity state. A 20% change in relaxation rate is observed through the removal of a H_2O blocking group, increasing *q* and, thus, improving inner sphere T_1 relaxation (Fig. 2). Since then, several similar approaches have been published describing the modulation of MRI contrast through the control of water access to a chelated paramagnetic centre.[29-31] These have achieved 3-fold increases in relaxation rate upon enzymatic cleavage of the hydration-hindering group.[29] An alternative approach has been offered by Giardiello *et al.*, who prepared a neutral complex that binds with high affinity to H_2O-blocking HCO_3^- anions and displays low relaxivity. The action of a specific enzyme (porcine liver esterase) on the modified side arms of this DOTA derivative introduces new anionic charge, repels the chelating HCO_3^- ions increases metal hydration, and triggers a ~90% increase in signal contrast.[32] Reliance on inner sphere hydration as the mechanism of MRI contrast modulation, however, is not ideal. Anion interactions with the cleaved (more solvated/accessible) paramagnetic species, has, in particular, been identified to be a considerable interfering factor, particularly *in vivo*, where water-competing anions are abundant.[30] Such interactions can have a significant detrimental effect on resulting relaxivity and any assumptions therein; alternative mechanisms to achieve MRI activation have, therefore, been investigated.

One such mechanism is the so-called receptor-induced magnetisation effect (RIME), which utilises binding of a target moiety, such as a protein, to a paramagnetic chelate, resulting in the formation of a bulky, slow-tumbling macromolecular contrast agent with increased τ_R (and thus relaxation/contrast relative to background; Fig. 3).[33] In this vein, Breckwoldt *et al.* have employed a bis-5-hydroxytryptamide-diethylenetriamine-pentatacetate gadolinium species, which, in the presence of the enzyme myeloperoxidase (MPO, a key enzyme secreted in the inflammatory response to tissue injury), oxidises and radicalises, leading to cross-linking, polymerisation and subsequent protein binding.[27] Successful triggering of relaxation enhancement was non-invasively monitored *in vivo*, allowing tracking of MPO activity in stroke-affected mice models. A Gd^{3+}-diethylenetriaminepentaacetic acid (DTPA) type construct with a phosphonate side-chain, termed MS-325 by Caravan *et al.*, which targets human serum albumin (HSA), again employs the RIME strategy to provide selective vascular MRI enhancement. In this case, HSA binding limits extravasation of the free chelate from the blood pool into the non-vascular space, slowing renal excretion and contributing to an extended blood half-life and also thus providing vascular-specific relaxation rate enhancement. A 9-fold increase in relaxivity (at 20 MHz) was observed upon non-covalent HSA binding in *ex situ* studies, due to slowing molecular rotation (τ_R) of the

HSA-bound MS-325 entity.[33] A similar strategy employs a Gd^{3+}-chelate functionalised with a trilysine masking group with associated poor native HSA affinity (and hence low relaxivity, r_1 = 9.8 mM^{-1} s^{-1} at 20 MHz, 37 °C). Upon cleavage of the lysine residues by human carboxy peptidase B, a thrombin-activatable fibrinolysis inhibitor (TAFI, an important enzyme in thrombotic disease), the chelate–HSA affinity increases substantially due to the exposure of aryl groups with high HSA binding affinity, a transition with an associated 170% relaxivity enhancement (to 26.5 mM^{-1} s^{-1} at 20 MHz, 37 °C).[34] Sherry and co-workers have designed a Gd–DO3A-peptide-based CA that is τ_R activated upon binding to a specific target protein in a similar vein.[35] The relaxivity of this CA (r_1 = 8.3 ± 0.2 mM^{-1} s^{-1} at 20 MHz) increases substantially upon addition of the target protein and phantom T_1-weighted imaging demonstrates a 10-fold improvement in image intensity for the chelate in the presence of the binding protein. More recently, Gd^{3+}–DO3A ligands bearing a pendant diphenylphosphinamide arm have been shown to possess a high affinity for HSA, boosting r_1 by 54–119% due to increases in τ_R.[36] The degree of relaxivity switching, however, was adversely affected by the displacement of inner sphere water molecules by carboxylate residues of the protein, an inherent problem often observed in the presence of oxygen-based chelates.

The vast array of diagnostically potent functional enzymes and proteins present physiologically makes this class of bioresponsive CAs arguably the most important in detecting and monitoring disease pathology. The examples of bio-responsive switchable CAs referred to herein represent some of the most effective (in terms of the degree of switching) of this class so far available and exploit robust change in q or τ_R. It should be highlighted, however, that the majority of these cases present irreversible changes in contrast, with a ‘one-off’ trigger facilitating the contrast enhancement or reduction. Further work will be required to generate derived CAs capable of long-term use or disease treatment profiling.

2.3 Cation responsive molecular contrast agents

Another important class of biologically activatable CAs are those which can be triggered by the presence of metal ions. Metal ions are vital in a variety of physiological pathways. Ca^{2+} ions for example, play an important role in neural signalling and changes in brain activity can lead to variations in its concentration. Similarly, increased Zn^{2+} ion concentrations have been implicated in environments commonly associated with Alzheimer’s disease.[37] Cation responsive contrast would therefore undoubtedly be diagnostically potent.[38] In the design of such, signal changes are once again most commonly effected through variance in hydration number of paramagnetic CA complexes. There have been several examples exploiting this in recent literature, most of which employ conformation changes and associated perturbations in inner-sphere water access and q. The first reports of a Zn^{2+}-specific CA reporter were by Hanaoka *et al.*, who described DTPA–bisamide chelators which respond sensitively and selectively to Zn^{2+} through the displacement of inner sphere water arising from a Zn^{2+} binding induced geometrical reconfiguration.[39,40] Such systems observed a ~33% decrease in relaxivity due to the inhibition of water access to the Gd^{3+}-chelator upon cation binding. Gadolinium complexes with bis-15-crown-5 ether or β-diketone recognition sites have also been prepared to enable the detection of K^+, Mg^{2+} or Ca^{2+} ions, with MRI signal contrast

again decreasing due to a geometrical rearrangement in the presence of the metal ion, and associated change in the second sphere of paramagnet hydration.[41] Within this study, the most efficient MRI response was observed for β-diketone tethered Gd–DTPA species, whose r_1 relaxivity (4.98 mM^{-1} s^{-1} at 20 MHz) decreased 20.7% (to 3.95 mM^{-1} s^{-1}) in the presence of Mg^{2+} ions.

These modulations, based on decreases or 'turning-off' of image contrast, are less desirable than systems which result in image brightening through specifically triggered relaxivity increase. Groups such as that of De Leon-Rodriguez and co-workers have prepared Gd^{3+}–DOTA chelates appended with *N*,*N*-bis-(2-pyridylmethyl) ethylene diamine (bisBPEN) diamide functionalities which are capable of binding Zn^{2+}. Such species successfully exhibit a modest ion-specific increase in r_1 relaxivity of 20% (from 5 to 6 mM^{-1} s^{-1} at 23 MHz) with the introduction of 2 equivalents of Zn^{2+} ions (with similar changes observed in the presence of Cu^{2+} ions).[42] These changes were attributed to an increase in water exchange rate upon ion binding, or alternatively, the creation of a more organised second sphere of water molecules (bound to the Zn^{2+} or Cu^{2+} ions) in close proximity to the single Gd^{3+}-bound water molecules of the complex. This group has recently improved upon this by using a Gd–DOTA derivative containing two bis-(3-pyrazolyl) units, yielding a 64% relaxivity enhancement with introduction of Zn^{2+} ions, also demonstrating successful *in vivo* application.[43] Interestingly, these groups also describe significant further r_1 relaxation enhancement of the Zn^{2+}-coordinated complex upon binding to human serum albumin (HSA), providing a 165% increase (from 6.6 to 17.4 mM^{-1} s^{-1}), a rotational correlation time (τ_R) effect only occurring in the presence of the metal ions.[42] Major *et al.* have demonstrated that the design of the chelate species can play a vitally important role in relaxivity modulation by specific cations.[44,45] Their asymmetric chelates display an acetate pendant arm capable of switching its coordination to either the paramagnetic centre of the contrast agent or a cation, such as Zn^{2+}. Coordination to the former centre generates a coordinatively saturated chelate, with $q = 0$ and hence low MRI contrast. Coordination to a Zn^{2+} ion causes a change in the molecular geometry and the Gd^{3+} coordination sphere, leading to an increase in hydration number to $q = 1$ (Fig. 4), and 121% increase in r_1 relaxivity (from r_1 = 2.3 to 5.1 mM^{-1} s^{-1} at 60 MHz). Subsequent *in vitro* studies demonstrated a qualitative increase in T_1-weighted image contrast of the agent in the presence of physiologically relevant concentrations of Zn^{2+}.[44]

Specificity amongst metal ions can, of course, be an important factor for consideration in the design of metal ion-modulating MRI contrast. Gd-chelates have been designed to recognise various different metal ions, including Cu^{2+}, Ca^{2+}, Mg^{2+} and K^+ with selectivities generally utilising Irving-Williams governed trends in affinity as well as coordination environment preferences.[46] Ethylene glycol tetraacetic acid (EGTA, a highly selective Ca^{2+} chelator) has, for example, been bound to two macrocyclic Gd^{3+}-containing moieties, with Ca^{2+} ion binding causing increases in the inner-sphere hydration number of the chelate and concomitant modest associated protic longitudinal relaxivity increases (32% from r_1 = 5.4 to 7.1 mM^{-1} s^{-1} at 500 MHz).[46] Similar constructs exploiting *q* to effect a contrast change have shown 83% increases in relaxivity in the presence of Ca^{2+} (from r_1 = 3.4 to 6.3 mM^{-1} s^{-1} at 500 MHz); at physiological concentrations, such as those in the relevant range for

Ca^{2+} modulation in the brain (0.8–1.2 mM), relaxivity changes of ~10% are observed.[47] Similarly, DOPTA–Gd complexes structurally modulate inner-sphere water access to the chelated Gd^{3+} ion using iminoacetate arms, which shield the paramagnetic centres from water in the absence of Ca^{2+} ions ($q = 0$).[48] Upon binding of Ca^{2+}, the complex undergoes a reorganisation leading to an increase in q and relaxivity by 80% to 5.8 mM^{-1} s^{-1} (at 500 MHz) over Ca^{2+} concentrations ranging 0.1–10 μM. Cu^{+}/Cu^{2+} ion selectivity has been achieved by Que *et al.* through the design of Gd–DO3A chelates coupled to acetate or thioether-rich receptor ligands, which rely upon modest q modulation through Cu^{2+} binding (eliciting a 40% change in relaxivity).[49,50] Similarly, Pope and co-workers use a bis-macrocylic ligand which recognises Hg^{2+} to generate a 24% increase in relaxivity.[51] The highest increase in longitudinal MRI relaxation exploiting a hydration change mechanism has been observed for thioether-tethered DO3A chelates, demonstrating a 360% increase in r_1 upon binding 1 equivalent of Cu^{2+} (from 1.5 to 6.9 mM^{-1} s^{-1} at 20 MHz).[50] The initially low r_1 observed in the absence of metal ions in this work is suggestive of a $q = 0$, with the acetate or pyridine moieties present on the linker initially capping inner-sphere water access (a cap that is removed on the association of Cu^{2+} ions; Fig. 5). A polyarginine modified version of this chelate has demonstrated some promise in initial intracellular work.[52] Recently, several others have reported a variety of Gd–DOTA-based chelates with pendant arms capable of cation binding, providing relaxivity responses due to q modulation.[53-55]

Modulation of MRI contrast based on metal ion recognition by a CA can also be achieved through exploitation of rotational correlation time. Peters and co-workers have investigated bisphosphonate appended coordination oligomers of a DOTA-like chelator as a means of generating cation triggered changes in rotational correlation time.[56] This resulted in 200–500% increases in r_1 (depending on Zn^{2+} concentration), although it was noted that selectivity would be poor under physiological conditions. A 250% relaxivity enhancement of Gd–DOTA–diBPEN in response to Zn^{2+} ions has recently been translated reasonably well to both *ex vivo* and *in vivo* studies, an effect which relies upon binding of the Zn^{2+}-bound-chelate species to HSA and resulting changes in τ_R.[57] Several groups have investigated heterometallic complexes featuring Gd-chelates which self-assemble to form bulky macromolecules upon coordination to iron ions.[58-61] Comblin *et al.*, for example, have designed a Gd(phen)HDO3A chelate (r_1 = 3.7 mM^{-1} s^{-1} at 20 MHz) which uses its phenanthroline-like unit to complex Fe^{2+} ions, forming a tris-complex with very high molecular weight, with an associated relaxivity increase to 12.2 mM^{-1} s^{-1}.[11] Toth and co-workers have developed a metallostar structure comprising six densely packed Gd^{3+}–diethylenetriaminetetraacetic acid (DTTA) chelates around an Fe^{2+} ion, resulting in an almost 2-fold increase in relaxivity (from 12.4 to 20.2 mM^{-1} s^{-1} at 20 MHz).[59] The formation of slowly rotating macromolecular species with increased τ_R is responsible for the observed enhancements throughout all these works. An alternative method for metal ion detection employing relaxivity responses which has been explored by Muller *et al.* describes the transmetallation of a DTPA-derived chelate (MS-325) which releases Gd^{3+} into solution in the presence of Zn^{2+} ions, resulting in insoluble Gd–phosphate complexes which precipitate and hence no longer contribute to the observed ^1H r_1 relaxivity.[62] This process leads to a 25% reduction in r_1 after 5000 min. The timescale and associated toxicity risk of this method, however, is unlikely to make it practically relevant.

There have been, then, a number of reported approaches to tune r_1 relaxation through association with physiologically relevant levels of cations. In nearly all cases this has been through the modulation of water access or rotational correlation time and accompanied by varying degrees of relaxivity switching (20–360%). Bar some obvious exceptions, performance is both modest and detrimentally affected in attempts to extrapolate to physiological *in vivo* conditions. Though much work clearly remains to be done, particularly in safeguarding specificity, these prior reports show promise and are likely to underpin future developments.

2.4 pH-responsive molecular contrast agents

MRI contrast agents capable of detecting variations in environmental pH can be of particular use for the non-invasive detection of disease or metabolic disorder.[63] Ischemia, for example, is often defined by low pH (caused by amide exchange due to regional neural ischemia, for instance) and can characterise heart disease. Similarly, regions of acidity can indicate the presence of hypoxia, tumour growth and metastases (malignant tumours present with pHs ranging from 6.8–7.2).[64] pH reporters can hence provide important information which can impact directly upon selected treatment (*e.g.* hypoxic tumour cells are resistant to radiation and to many anticancer drugs[65]) and a monitoring of their efficacy. It is unsurprising then that a range of paramagnetic agents have been developed in which hydration state, leading to either increases or decreases in signal, is highly pH dependent.

Pagliarin and co-workers have, for example, described a series of Ln^{3+} macrocyclic complexes in which the presence of a β-arylsulfonamide group on the chelate species supports pH dependent relaxivity (as well as luminescence).[16] These systems are based on protonation of the sulphonamide nitrogen and the associated increase from $q = 0$ to $q = 1$ (with a 48% increase in r_1 relaxivity values over the pH range 7.4–6.8 and concomitant decrease in photoluminescent emissivity due to water based quenching). Hall *et al.* have synthesised terpyridine-based Gd^{3+}-chelates which demonstrate decreasing relaxivities with increasing pH (from $r_1 = 12.8\ mM^{-1}\ s^{-1}$ at pH 6 to $r_1 = 2\ mM^{-1}\ s^{-1}$ at pH 11, at 20 MHz), attributed to an overall decrease in q from 3 to 0, due to the successive deprotonation of water molecules and subsequent formation of dimeric complexes possessing no bound water molecules.[66]

An alternative approach to pH modulation of MRI is to exploit proton exchange between inner sphere coordinated water molecules and bulk water due to highly acidic/basic environments. This approach has been employed by Aime *et al.*, who have described a range of C_4-symmetric Gd^{3+}–DOTA-type chelates with different pendent arms demonstrating largely invariant relaxivity between pH 2–8 (where $r_1 \approx 2.5\ mM^{-1}\ s^{-1}$ at 20 MHz, due to only outer-sphere contributions), but marked increases in r_1 at very high (>10; $r_1 \approx 5.7\ mM^{-1}\ s^{-1}$ at 20 MHz) and very low (<2; $r_1 \approx 5\ mM^{-1}\ s^{-1}$ at 20 MHz) pH environments.[22,23] The observed increases in relaxation behaviour at these two extremes are attributed to the formation of a well-defined second hydration sphere, where water molecules are in rapid exchange. In strongly basic media this is ascribed to deprotonation of bound water molecules or proximate ligand amide NH protons. In acidic media these beneficial changes are ascribed to protic-catalysed dissociation of the ion-paired water–Gd-

complexes, promoting water exchange. Similar work by Sherry and co-workers has described Gd^{3+}–DOTA complexes with phosphonate pendent arms with strong pH-dependent r_1 behaviour, demonstrating two relaxivity troughs, the first having a 40% variation between pH 2–6 and 70% between pH 6–12, with an r_1 maximum at pH 6, observations again ascribed to protic exchange between bound water protons and bulk solvent protons contributing to a second hydration sphere possessing rapidly exchanging water molecules.[24,25]

A major limitation inherent in the field of responsive contrast lies in the lack of ability to quantify the concentration of contrast agent present at the site of interest (meaning, in turn, that relaxivities resulting from any trigger can only be qualitative). There is, then, much interest in the development of ratiometric responsive CAs and most development thus far has been associated with those which respond to local pH. Sherry and co-workers have, for example, investigated such a system (employing a mixture of pH-insensitive $GdDOTP^{5-}$ and pH sensitive $GdDOTA\text{-}4AmP^{5-}$ chelates with necessary assumptions about identical biodistribution) and demonstrated its efficacy both *in vitro* and *in vivo*.[17,67] An alternative approach is to measure the ratio between the transverse and longitudinal paramagnetic relaxation rates of water protons in response to a single contrast agent (R_2/R_1), as described by Terreno and co-workers.[68] This approach, based on a Gd^{3+}-complex having τ_m or rotational mobility dependent on pH, allows an assessment which is independent of contrast agent concentration. Bimodal agents employing a second imaging technique using a dual-functional probe can also provide quantification of local contrast agent concentration and hence relaxivity,[69] an approach adopted in work by Frullano *et al.*, which saw the production of a dual MRI-PET agent composed of the pH-dependent GdDOTA-4AMP chelate appended with a $^{18/19}F$ functionality.[70] A linear relationship between the PET and MRI signals allowed determination of the concentration of the agent through comparison with a pH calibration curve, providing a quantitatively accurate non-invasive probe of great promise for *in vivo* application.

To summarise thus far, the most common and controllable approach to effect relaxation change by pH modulation is through exploitation of the hydration state (q) of molecular contrast agents. In this way, enhancement or reduction of signal contrast can be attained, with modest (up to 70%) changes over relevant physiological pH ranges (pH 6–8).[24] The use of protic exchange and second hydration sphere dynamics can provide an alternative pH responsive route to MRI contrast modulation, although the most significant responses occur at very high (>10) or very low (<2) pH regions, making such responses less physiologically relevant. To allow unambiguous assessment of MRI contrast modulation, the contrast agent concentration must be accurately known, a particularly difficult prospect in site-targeting and *in vivo* applications. Responsive ratiometric contrast agents offer great potential in this area and some initial investigations have demonstrated promise.

2.5 Redox responsive molecular contrast agents

Redox reactions are widespread in biochemical systems, with organisms integrating them directly within fundamental methods of energy generation. A change in oxidising/reducing condition can result from variations in blood flow, oxygenation and other variables and can

have a profound effect on physiological function, such as those in the brain accompanying stroke, Parkinson's and Alzheimer's diseases.[71] Very often such physiological stress is associated with increased reactive oxygen species (ROS) and decreased antioxidant levels.[72,73] One can seek to directly acquire tomographic mapping of such conditions through the use of paramagnetic agents which are, in some capacity, redox active.

One non-metallic class of such are the nitroxides, which undergo reduction to diamagnetic hydroxylamines, resulting in a marked and reversible contrast change.[71,73] These aside, T_1-weighted contrast agents demonstrating redox triggered contrast switching are rare.[74-76] Louie and co-workers have described the only Gd^{3+}-based T_1-contrast agents capable of redox sensing using a Gd^{3+}–DOTA system featuring a spiropyran/merocyanine motif, demonstrating 26% relaxivity decreases upon redox activation (from 2.5 to 1.9 mM^{-1} s^{-1} at 60 MHz), caused by decreasing hydration number (from q = 1.16 to 0.44) as a result of a conformation change.[74,75] An 8-coordinate chelate complex tethered with acyclic merocyanine converts to its spirocyclic isomer, a 7-coordinate chelate, following reduction using nicotinamide adenine dinucleotide (NADH). This structural change increases the hydration number of the complex (from q = 1 to q = 2), resulting in a 54% increase in relaxivity; a change which is reversible upon treatment with hydrogen peroxide (Fig. 6).[74]

A slightly different mechanistic approach has also been explored towards the development of redox switchable CAs sensitive to environmental O_2 partial pressure (pO_2, which is relevant in various pathological diseases, including stroke and tumours), exploiting variations in the chelate metal centre oxidation state, similar to the BOLD method of activated detection earlier described.[77] In this vein, Terreno and co-workers have investigated manganese ($Mn^{2+/3+}$) porphyrin complexes which were encapsulated into cyclodextrin (CD) hosts.[78] Oxidation of Mn^{2+} complexes to Mn^{3+} by O_2 was associated with ~50% decreases in MR signal intensity (r_1 = 5 mM^{-1} s^{-1} to 2.5 mM^{-1} s^{-1} at 20 MHz); changes attributed to a combination of electron spin density delocalisation and changes in the number of labile protons at the metal centre.[78-80] This system allows quantification of pO_2 (0–40 Torr) in the region of interest. Some Eu^{2+} analogues have also been investigated as potential redox-responsive probes, due to their isoelectronic relationship with Gd^{3+}. Burai *et al.*, for example, have investigated chelates based on cryptates, which, although not experimentally verified, have potential for strong redox triggered MRI contrast switching capabilities upon oxidation of Eu^{2+} to Eu^{3+}.[77,81]

Though there exist, then, a number of elegant examples of redox responsive MR contrast which have been applied *in vitro*, it is clear that much more work needs to be done before the realisation of reliable and marked switching of signal contrast *in vivo*.

2.6 Light responsive molecular contrast agents

Bioluminescence imaging is a useful non-invasive modality providing potentially excellent signal-to-noise, spatial refinement and high throughput. Although poor tissue penetration makes it a less tractable means of switching contrast than other methods noted thus far, light emitting gene markers, such as those based on lucerase–luciferin could potentially provide an appropriate application for photoactivatable agents.[21,82] To this end, a small number of articles have hence described the development of light-sensitive MRI contrast agents based

on spirobenzopyrans, which undergo an isomeric conformation change upon light irradiation, affecting water coordination (*q*) at the paramagnetic metal centre.[21,75] This transformation (which is reversible) prevents hydration at the metal centre, resulting in a reduction in relaxivity of about 21% (from r_1 = 3.7 mM^{-1} s^{-1} to 2.9 mM^{-1} s^{-1} at 60 MHz).[75] Though modest, this work may find application if, for example, larger relaxivity changes can be married with NiR wavelength triggering.

3. Macromolecular and nanoparticle contrast agents

Small molecule CAs have paved the way for enhanced medical imaging (including that which is targeted and/or multimodal), and facilitated most of what we understand in terms of tuning CA behaviour *in vitro* and *in vivo*. However, their limitations, in particular rapid elimination, and the quest for signal amplification, have resulted in the increased utilisation of higher molecular weight species offering inherently striking and, in many cases, profoundly advantageous characteristics.[13]

Relaxivity can be improved by the incorporation of paramagnetic gadolinium centres directly into a nanosized matrix to obtain, for example, GdF_3:CeF_3 nanoaggregates coated with poly(acrylic acid) chains,[83] doped zeolite GdNaY,[84] gadofullerenes,[85] gadonanotubes,[86] GdF_3:citrate,[87] or PEG–phosphate coated $NaGdF_4$ nanoparticles.[88] Though a number of these derivations are associated with high MR contrast, they very often exhibit low kinetic stability and hence potentially high levels of toxicity. A preferred method of increasing signal contrast is by embedding or conjugating numerous clinically approved Gd^{3+}-chelates to macromolecules or nanoparticulates based on polymers,[89] dendrimers,[90] liposomes,[91] micelles,[92] proteins,[93] virus capsids,[94] gold glyconanoparticles,[95] or silica.[96] These approaches primarily exploit the inherently large particle surface area and size to improve MRI signal. Before looking at some of the characteristics associated with the paramagnetic modification of such species, we briefly review the mechanisms associated with the dipole–dipole longitudinal relaxation mechanism. As outlined earlier (eqn (3) and (4)), inner-sphere contributions generally dominate relaxation enhancement. The longitudinal relaxation rate of the bound water ($1/T_{1m}$) is given by eqn (5). These expressions confirm that the relaxation behaviour of a complex depends on a number of parameters, including the distance between the unpaired electron spin of Gd^{3+} and protons of the coordinated H_2O (r_{Gdh}), the angular proton Larmor frequency (ω_I) and the global and local correlation times (τ_{CG} and τ_{CL}, respectively, defined by eqn (6) and (7)).

$$\frac{1}{T_{1\mathrm{m}}}=\frac{2}{15}\left(\frac{\mu_0}{4\pi}\right)^2\frac{{\gamma_\mathrm{I}}^2 g^2 {\mu_\mathrm{B}}^2 S\left(S+1\right)}{{r_\mathrm{GdH}}^6}\left[\frac{3F^2\tau_{\mathrm{CG}}}{1+{\omega_\mathrm{I}}^2{\tau_{\mathrm{CG}}}^2}+\frac{3\left(1-F^2\right)}{1+{\omega_\mathrm{I}}^2{\tau_{\mathrm{CL}}}^2}\right] \quad (5)$$

$$\frac{1}{\tau_{\mathrm{CG}}}=\frac{1}{\tau_{\mathrm{m}}}+\frac{1}{\tau_{\mathrm{RG}}}+\frac{1}{T_{1\mathrm{e}}} \quad (6)$$

$$\frac{1}{\tau_{\mathrm{CL}}}=\frac{1}{\tau_{\mathrm{CG}}}+\frac{1}{\tau_{\mathrm{RL}}} \quad (7)$$

where μ_0 is the permeability of vacuum ($\mu_0 = 1.257 \times 10^{-6}$ N A^{-2}), γ_I is the gyromagnetic constant for protons ($\gamma_I = 2.675 \times 10^8$ T^{-1} s^{-1}), g is the electronic g-factor ($g = 2$), μ_B is the Bohr magneton ($\mu_B = 9.274 \times 10^{-24}$ J T^{-1}), S is the total electron spin of the material ion ($S = 7/2$ for Gd^{3+}), F^2 denotes the order parameter (*vide infra*) and T_{1e} is the electron spin longitudinal relaxation time.[97]

As a result of the natively increased steric bulk of nanoparticles or macromolecules, tumbling of the appended molecular paramagnetic probe is, relatively, slowed down; the associated increase in overall rotational correlation time (τ_R) providing concurrent improvement of relaxivity.[98] The length of τ_R for small molecular weight Gd^{3+}-chelates is in the picosecond range (50–200 ps),[99] 1–3 orders smaller than τ_m and T_{1e}, and so τ_C is dominated by τ_R.[100] On the other hand, τ_R of their higher molecular weight counterparts is in the nanosecond range (0.5–50 ns), a timescale which is comparable or even longer than τ_m and T_{1e}. Since eqn (4) predicts a higher relaxivity for a shorter τ_m value ($\tau_m << T_{1m}$) and T_{1m} can already be more than one order of magnitude shorter in such systems (eqn (5) and (6)), the relaxivity of nanoparticulate contrast agents is characteristically limited by rather long τ_m and thus slow k_{ex} ($k_{ex} = 1/\tau_m$).[97]

An important consideration in the design of macromolecular or nanoparticulate CAs with high relaxivity is the structure and flexibility of the linking moiety (it is not necessarily the case that the particle structural rigidity and rotational time are directly translated to appended complexes). Fast rotation around the Gd^{3+}-complex linker compared to the motion of the nanoparticle can be a limiting factor in the relaxivity enhancement; if Gd^{3+}-complexes are covalently attached to the surface of the particle through a flexible linker, their local rotational motion (τ_{RL}) around the axis of the linker in solution is much faster than the global rotation of the nanoparticles (τ_{RG}) (Fig. 7). Using the Lipari–Szabo approach[85,86] incorporated into the SBM equations, the relaxation parameters of nanoparticulate MRI probes can be obtained through fitting of experimental nuclear magnetic resonance dispersion (NMRD) profiles.[101] The degree of spatial restriction of the motion, *i.e.*, the extent to which τ_{RL} and τ_{RG} contribute to τ_R is described by the order parameter F^2 ($0 \leq F^2 \geq 1$). If τ_{RL} is negligible, as in a perfectly rigid system, F^2 equals 1. In more conformationally flexible environments, F^2 approaches 0, and internal motions are completely independent of global motion.[96] These nanoscale effects are summarised in eqn (5), which is valid at $B_0 > 1.5$ T if the global molecular reorientation is isotropic.[3,97]

This theoretical framework enables evaluation of the rigidity and the internal motions of the nanosized system, the influence of the length and flexibility of the contrast agent linker on the relaxation parameters, and the contributions emerging from both the appended molecular MRI probe and from the nanoparticle to the overall relaxation of the composite.[102] The number of nanoparticulate-based MRI contrast agents has rapidly increased in recent years, due not only to their capacity to deliver a large number of paramagnetic ions per nanostructure, allowing improvements in relaxivity per unit dose compared to individual Gd^{3+}-chelates, but especially, as noted, due to their ability to boost relaxivity by retarding the chelate tumbling rate.[98]

The conjugation of Gd^{3+}-chelates to block, graft, or micellar macromolecular carriers generates a class of CA whose relaxivity is dependent on the polymer rigidity.[90,103] This, in turn, is chemically tuneable through the overall molecular weight,[104] by the incorporation of monomers with high glass transition temperatures,[105] by grafting of conjugated polymers possessing a more rigid backbone,[106] enhancing the degree of cross-linking,[107] lengthening and making side chains hydrophobic,[102] or by increasing the number of internal hydrogen bonds (and hence reducing internal motion).[90] Improved H_2O exchange can be achieved by the incorporation of a hydrophilic shell layer that serves as a reservoir for water molecules.[108] On the other hand, grafting polyethyleneglycol (PEG) chains onto hyperbranched polymers and dendrimers is known to slightly decrease relaxivity because of hindered water exchange.[103,109] In dendrimers, relaxivity can be maximised with each increase in branching generation, through τ_R effects. This trend, however, is not exhaustive and has been found to decrease once the G9 generation is reached.[13] Macromolecular formulations with an MRI sensitivity that is environmentally responsive in a simple manner can be achieved by selecting monomers with responsive functional groups,[110] by gating the water accessibility,[111] by conformational conversion between globular and extended form,[107] through the incorporation of cleavable linkers,[103] and by switching between hydrophobic interaction and electrostatic repulsion,[112] amongst others.

Cone-like or truncated cone-like amphiphiles that self-aggregate into micelles or liposomes under specific conditions have also been utilised to improve CA relaxivity.[13,97] Memsomes (Fig. 8) are a class of liposomes, where a paramagnetic complex can be attached to the hydrophilic heads of the lipid molecules in the bilayer, allowing easy access to solvent.[13] In this case, the attachment of the paramagnetic complex to the membrane is not rigid ($\tau_{RL} << \tau_{RG}$), and so the size of the memsome itself has no effect on relaxivity.[113] Instead, the latter is observed to be dependent on the rotational diffusion of the Gd^{3+}-complex on the surface of the liposome,[114] as well as on the length of the linker, tuning water accessibility to the lanthanide CA centre.[115] On increasing the alkyl chain length from C10 to C18, τ_{RG} can increase from 500 to 2800 ps. However, the advantage of high τ_{RG} is reduced in all liposomal systems due to the high internal mobility of the Gd^{3+}-complexes (short τ_{RL} and low F^2), and slow k_{ex}.[102] The latter is highly dependent on the phospholipid membrane's water permeability in enosomes, which comprise a group of liposomes that encapsulate water-soluble Gd^{3+}-chelates.[97] Enhancement of the permeability concomitant with a shortened τ_{io} (*i.e.* water exchange time between internal, i, and external, o, parts of the liposome)[116] can be achieved by increasing the temperature towards the phase transition temperature (T_M) that causes phospholipids to undergo a gradual increase in fluidity. In this system, quenched r_1 can only be recovered when the liposome composition allows for rapid water exchange between the interior and exterior of the enosomes ($\tau_{io} << T_{1i}$). Subsequently, relaxivity of the paramagnetic agent encapsulated within the liposome becomes similar to that in the solution. Higher concentrations of metal chelate encapsulated within the liposome and higher internal viscosity, further lengthens the rotational and diffusional correlation times, contributes to a slightly higher relaxivity compared to non-encapsulated Gd^{3+}-complex.[91,116]

Another important class of highly tuneable nanoparticulate CAs consists of inorganic biocompatible Gd^{3+}-chelate decorated mesoporous silica nanoparticles (MSNs) with uniform mesopore compartments and large silanol surface areas.[94,117,118] The geometric confinement of the former increases τ_R of the paramagnetic complex and τ_D of water molecules (increasing the H_2O–lanthanide interaction time) and, through this, relaxivity.[85,119] The tuneable surface chemistry can be further exploited to improve the accessibility of water and increase the water-exchange rate, k_{ex}. For example, a threefold faster k_{ex} was reported after acetylation of surface amine groups otherwise used for conjugation to Gd^{3+}-chelates.[120]

It is clear, then, that nanostructured and macromolecular materials can provide improved MRI signal contrast due to their behaviour in suspension. Such materials can be further engineered to offer stimuli responsive contrast in a predictable and useful manner. Their characteristics can be tuned through design and synthesis in terms of q,[121] τ_{RL},[122] τ_{RG},[89], τ_{io}[123] or τ_m,[114] and have the capability to additionally provide specificity to a site of interest, high *in vivo* mobility, and multimodality as well as multifunctionality. As such, they represent an increasingly important class of MRI contrast agent.

3.1 pH-responsive particulate contrast agents

Nanoparticulate MRI probes can be designed to exhibit significant contrast response to physiological or pathological pH change in the region of interest.[124] Most typically, this is through the incorporation of pH-responsive Gd^{3+}-chelates,[125] acid labile linkers such as ketals[126] or pH-responsive groups into a nanoparticle scaffold,[127] whose pH-responsiveness triggers a global response across the particle, such as a change in hydration state (leading to swelling/collapse), propensity to degrade/dissolve, hydrophilic/hydrophobic change, hydrodynamic diameter, conformational change (globular/linear), micellisation, or change in water permeability. These changes can result in marked changes in F^2,[112] q,[128] or τ_m,[68] and thus T_1 contrast.

Such structural changes are, of course, markedly more useful if the responsive functional groups possess pK_a values around physiological pHs (frequently employed groups which affect the hydration state q as a result of a response to a stimuli, include arylsulfonamide,[16] imidazole,[124] nitrophenol,[129] and phosphonate[125]). Aime and co-workers have, for example, reported an adamantane derivative of a sulfonamide based Gd^{3+}-chelate that was non-covalently hosted by a macromolecular carrier consisting of 8–10 poly-β-cyclodextrin units. With a pK_a of 6.7, the sulfonamide nitrogen deprotonates at basic pH and ligates to the metal centre, generating an “MRI silent” $q = 0$ state (a reversible change to $q = 2$ at acidic pH, ‘turning on’ relaxivity contrast). An additional integration into the same cyclodextrin scaffold of an adamantane functionalised ^{19}F-containing reporter can additionally engender ratiometric $^1H/^{19}F$ mapping of pH.[128]

On the other hand, anionic, pH-sensitive polymers, such as those based on polymethacrylic acid (PMMA), can accept or release protons (Fig. 9), resulting in swelling/contraction that modifies τ_R.[112] At pH 7, a Gd^{3+}–DO3A loaded spherical copolymer consisting of PMMA cross-linked by *N*,*N*′-methylenebisacrylamide becomes swollen due to electrostatic repulsion between the carboxy groups. At pH 4 carboxy group protonation induces the

formation of a compact globule conformation of restricted molecular motion and r_1 increases from 13.6 mM^{-1} s^{-1} to 28.0 mM^{-1} s^{-1}.[107]

The remarkably higher τ_R of a generation-5 poly(amidoamine) (G5-PAMAM) dendrimer loaded with Gd^{3+}–EPTPA in an acidic environment was studied in detail by Merbach and co-workers using the Lipari–Szabo approach to fit NMRD profiles. Under acidic conditions, repulsions between positively charged atoms associated with protonation of tertiary amines were increased, leading to an extended dendritic structure of slower global rotation (longer τ_R due to increased τ_{RG} = 4.04 ns) and increased hydrogen bond governed rigidity (F^2 = 0.43). The increases in τ_{RG} and F^2 above those noted at basic pH (τ_{RG} = 2.95 ns, F^2 = 0.36), generated relaxivity increases from 13.7 to 23.9 mM^{-1} s^{-1} at low pH.[90]

The opposite effect of pH on τ_R was reported for a macromolecular probe comprising 114 ornithine residues, 30 of which were linked to aminoethyl-functionalised Gd^{3+}–DO3A through a squaric acid moiety. At acidic pH, cationic terminal amine side chains were highly hydrated and repelling, generating a highly flexible structure of low τ_R and r_1. At basic pH, deprotonation of the amine groups led to formation of a rigid α-helix structure, with an associated increase in r_1 to 32 mM^{-1} s^{-1}.[131] This behaviour was consistent with increasing τ_R with pH as determined by NMRD. Above pH 7, the R_2/R_1 ratio was independent of the local concentration of the paramagnetic agent allowing ratiometric imaging.[132]

Both τ_m and τ_R contributed to responsiveness when 96 Gd^{3+}-chelate moieties, each with four pH-sensitive phosphonate pendant arms that form hydrogen-bonds with bulk water (phosphonate triggered protic exchange in the second-hydration sphere[133] is described in Section 2.3), were covalently coupled to a G5-PAMAM dendrimer by the group of Sherry. At pH 9, r_1 (10.8 mM^{-1} s^{-1}) was reportedly limited by slow water exchange. As the pH fell below 8.5, the phosphonates were consecutively protonated, and their effectiveness at catalysing proton exchange at Gd^{3+}-coordinated H_2O with bulk H_2O increased. The combined effects of faster inner-sphere water exchange, longer τ_m of the second sphere due to either a larger or more ordered second coordination shell (*via* protonated phosphonates), and longer τ_R as a result of protonation of amines within the dendrimer, (turning on hydrogen bond mediated rigidification),[90] increase r_1 to 24.0 mM^{-1} s^{-1} at pH 6. However, the ultimate relaxivity here was limited by relatively slow water exchange in the inner-sphere (in the microsecond range) and by relatively fast protic exchange in the second-sphere (in the nanosecond range).[134]

τ_m and τ_R have also been pH tuned through the loading of an amphiphilic Gd^{3+}–DO3A derivative bearing a sulfonamide moiety into large unilamellar vesicles (LUV). Subsequent relaxivity decreases at high pH were ascribed not only to changes in inner-sphere hydration of the Gd^{3+}-chelate (from q = 2 to q = 0), but also to its changed intraliposomal distribution and water exchange across the vesicle's membrane. In an acidic environment, protonation of the sulfonamide moiety with concomitant removal of the arm from the coordination cage of the Gd^{3+}-ion caused its incorporation deeper into the liposomal membrane. As a result, the increased number of Gd^{3+}-complexes intercalated into the membrane led to a higher τ_R with respect to the free complex, an elongated τ_m, an increased membrane permeability to water and consequently an enhanced relaxation rate R_1. In a rather unusual step, the authors finally

report that, in mapping the dependence of the ratio of the ^{1}H R_1 relaxation rates at two different magnetic fields (40 MHz and 8.5 MHz) on pH (Fig. 10) ratiometric pH MR imaging can be achieved (image contrast independent of CA concentration).[135]

There are, then, several different approaches which can be employed in the generation of high r_1 CAs with pH sensitive contrast. The most common approaches utilise either pH dependent swelling, causing variations in τ_R, or pH dependent metal hydration/water exchange rate. In most cases, relatively modest (~2-fold) changes in relaxivity have been achieved to date. The potential within this field, however, is vast, with a range of disease states triggering notable variation in local pH profile. This is likely to be an area of active publishing in the coming years.

3.2 Redox-responsive particulate contrast agents

In comparison to pH, there are relatively few examples of particulate-based T_1 MRI probes for which contrast is tuned through a redox event. To date, examples are primarily based on changes in rotational correlation time. For example, the redox-responsive relaxivity change of a nanoparticulate MRI probe based on a thiol/disulfide redox couple is caused by variation in molecular dynamics (τ_R) as a result of degradation. Nanocapsules based on several β-CD units linked by disulfide bridges incorporated Gd^{3+}-chelates that were able to interact with β-CD *via* hydrophobic pendant aromatic residues. The incorporated Gd^{3+}-chelates exhibited high relaxivity (15.2 mM^{-1} s^{-1} at 70 MHz) due to restricted mobility and good water permeability through the β-CD shell. The addition of a reducing agent caused the nanocapsules to disassemble, releasing the β-CD monomers and Gd^{3+}-complexes. As a result, τ_R was shortened and relaxivity decreased to 8.2 mM^{-1} s^{-1}.[136]

In comparable work but with converse observations, Liang and others obtained an enhanced relaxivity through elongated τ_R as a consequence of self-assembly of gadolinium doped nanoparticles triggered by enzymatic and reductive cleavage.[137] After entry into cancer cells, the disulfide bond of an MRI contrast agent (r_1 = 6.0 mM^{-1} s^{-1}) consisting of Gd^{3+}–DOTA, 2-cyanobenzothiazole and a peptide sequence containing an S–S bond, was reduced by glutathione and the peptide sequence cleaved by furin, a *trans*-Golgi protease overexpressed in tumours. The so-generated intermediate Gd^{3+}-complex condensed into an amphiphilic dimer with increased relaxivity (13.2 mM^{-1} s^{-1}), self-assembling *via* π–π stacking into gadolinium containing nanoparticles, with τ_R once again being responsible for contrast modulation.[138]

These examples demonstrate that effective relaxation responses can be observed using a redox stimulus, although reductions in relaxivity resulting from dissolution are less useful from a potential toxicity perspective, increases due to lengthened τ_R can provide >100% contrast signal enhancement.

3.3 Thermo-responsive particulate contrast agents

Temperature sensitive nanoparticulate MRI probes can potentially be used for both measuring temperature distribution in the human body, and thermometry, the latter largely

based on local hyperthermia for either chemodosimetry or controllably killing cancer cells.[123,139,140]

In terms of CA relaxivity, work to date has focused on either temperature induced release of Gd^{3+}-chelates from a liposomal core[140] or by a change in water access to particle internalised Gd^{3+}-complexes.[141,142] In both cases all prior work has been based on the transition of the liposomal phospholipid bilayer from a highly ordered gel-like phase that serves as a diffusion barrier to a fluid-like disordered state with increased membrane permeability (at $T > T_M$).[123]

Grüll and others have, for example, investigated liposomes consisting of several different lipids including a thermoresponsive 1,2-dipalmitoyl-*sn-glycero*-3-phosphocholine (DPPC, T_M = 41.5 °C[140]), and a lysolipid 1-palmitoyl-*sn-glycero*-3-phosphocholine (MPPC). T_1 measurements at $T < T_M$ imply that encapsulated Gd^{3+}-complexes remain inside the aqueous lumen of the liposome so that relaxivity is limited by the water diffusion across the bilayer. This increases with increasing temperature, such that there is a sharp reduction in T_1 (from 1828 ms to 394 ms) above the T_M, upon incubation of the liposomes at 45 °C for 30 min.[143]

In vivo studies were performed by Li *et al.*, who developed a DPPC-based thermo-sensitive liposomal formulation with encapsulated Gd^{3+}–DTPA and doxorubicin. Chelate release was triggered by local hyperthermia and quantified by MRI. T_1 relaxation of a tumour in a BALB/c mouse treated by such liposomes was 2878 ms. After hyperthermic treatment in a hot bath at 43 °C, T_1 was accelerated to 1509 ms in the rim (*i.e.* 1–2 mm band around tumour periphery) and to 2482 ms in the core of the tumour due to Gd^{3+}–DTPA release.[144]

A two-point thermometry system with an “off–on” and “on–off” transition using lipid nanoparticles containing P(NIPAM)-*co*-P(AM) crosslinked with a Gd^{3+}-chelate bi-linker was developed by Wu and others.[145] Poly(*N*-isopropylacrylamide) P(NIPAM) exhibits a unique temperature sensitivity, undergoing a reversible phase transition at 32 °C, expelling water and forming a contracted hydrophobic globule of low associated relaxivity.[146] The critical temperature of this transition could be raised with increasing amounts of copolymerised temperature insensitive monomer acrylamide (AM). At temperatures above the critical point the hydrophilic hydrogel containing the Gd^{3+}-chelate crosslinker was exposed to water, increasing T_1 signal.[145]

These investigations into the use of temperature activatable contrast agents exploiting tuneable interactions between bulk water and paramagnetic chelate have been successfully translated to *in vivo* studies and shown great promise,[144] particularly considering the demonstrable biocompatibility of the materials involved. Further analyses will undoubtedly present systems of greater control, tuneability and temperature definition.

3.4 Bio-responsive particulate contrast agents

Smart MRI nanoparticulate probes endeavour to sense molecular events, such as enzymatic activities and gene expression patterns at the level of the entire organism.[147] A number of attempts have been made to generate macromolecular contrast agents that respond significantly to the presence of a biomolecule of interest based on the so-called receptor-

induced magnetisation-enhancement (RIME) effect.[148] In many cases this has been achieved through a modulation of τ_R. Biotinylated DNA aptamers 3′ conjugated to Gd^{3+}–DOTA have, for example, been observed to switch the terminal r_1 relaxivity by ~40% in the presence/absence of adenosine. This sensing occurs through binding induced changes in DNA hybridisation with its associated change in steric bulk.[149] Similarly, T_1 contrast of a G5-PAMAM dendrimer conjugated to folic acid and Gd^{3+}-complex can be enhanced upon binding to a folate receptor due to resulting slower tumbling rates.[150] Similarly, the relaxivity of a gadolinium metallopeptide consisting of a DNA-binding transcription factor and a Ca^{2+}-binding moiety increased r_1 by 100% to 42.4 mM^{-1} s^{-1} at 60 MHz upon binding to DNA, due to an increased τ_R effect.[151] A τ_R dependent relaxometric procedure was also developed by Aime and others, who exploited a ratiometric couple based on Gd^{3+}–DOTA covalently linked to a peptide sequence and a lipophilic tail that was incorporated into a liposome (large R_2/R_1). As the matrix metalloproteinase-2 cleaved the sequence between serine and leucine, the gadolinium complex was released from the liposomal membrane, and, due to increased τ_R, R_2/R_1 was reduced by ~46% at 300 MHz independent of the total concentration of gadolinium.[152]

In addition, a Gd^{3+} complex itself can be responsive to direct ligation to a biomolecule, whereby the number of inner sphere bound water molecules q changes upon binding. This conceptually and chemically simple mechanism has, for example, been demonstrated with an octahedral nanocage consisting of four rigid tridentate ligands coordinating six gadolinium atoms that showed a r_1 of 388.5 mM^{-1} s^{-1}, at 400 MHz. Addition of glucosamine triggered a decrease in r_1 to 62.1 mM^{-1} s^{-1} due to substitution of coordinated water molecules and decreased q (selectivity over glucose was notably observed).[110]

Davis and co-workers have explored the first inorganic nanoparticle-based contrast system triggered by protein–protein recognition based on tuned water access and τ_m (Fig. 11).[111] They specifically reported the reversible contrast switching of Gd^{3+}-chelate doped MSNs (r_1 = 15.1 ± 0.57 mM^{-1} s^{-1} at 300 MHz) by tuning the water access to internally biased paramagnetic centres (and thus k_{ex}) using a surface immobilised protein of sufficient steric bulk (in the protein gated state r_1 = 5.8 ± 0.22 mM^{-1} s^{-1}). In the presence of a partner biomolecule (in this case a biotinylated protein), this steric cap was observed to be competed off, and both water access and high relaxivity were subsequently restored. This proof of principal serves to illustrate the significant potential of nanoparticle-based functional MR imaging in reporting on specific biorecognition processes.

The wide variety of potential bio-responsive triggers available which are associated with various disease and tumour states should stimulate further investigations into nanoparticle scaffolds, wherein both inherently high signal contrast and potentially dramatic contrast switching are possible.

4. Conclusions and future outlooks

There exist a plethora of MRI CAs which are capable of displaying strong positive or negative signals *in vitro* and *in vivo*. The prospect of CAs which can detect and respond to specific stimuli is an exciting one, with huge potential for non-invasive disease diagnosis

Europe PMC Funders Author Manuscripts

and, more generally, the (potentially whole body) “mapping” of local biochemistry. This article has focused on T_1 paramagnetic centre-based contrast agents, and described some of the mechanisms which can be exploited to facilitate change in MRI contrast signal in response to a specific environmental trigger (see Table 1). Molecular, macromolecular and particulate-based contrast agents can, specifically, be engineered such that variations in hydration number (q), rotational correlation (τ_R) or water exchange (τ_m) follow specific chemical or physical interactions with their environment.

In general, macromolecular and particle-based CAs provide higher relaxivity values than molecular agents alone, due in part to significant lengthening of the paramagnet rotational correlation times through its association with a rigid, bulky, species. The degree of relaxivity modulation observed, however, is, thus far, similar for both molecular and nanoparticulate agents (see Table 1). As protocols for the synthesis of homogeneous and well-characterised particles become widely used, this area is likely to develop markedly over the next few years. Tactics to facilitate response are likely to involve designed switching of τ_R and τ_m, as well as gating water access to encapsulated paramagnetic centres. The possibility of utilising additional (native or added) multimodal characteristics (nuclear or otherwise), high local concentrations and targeting would make these agents exceedingly powerful from a diagnostic perspective.

To date, it is clear that the chemical complexities of an *in vivo* environment often prove detrimental in keeping image contrast switches both substantial and selective. The development of improved particle characterisation methodologies together with chemistries that introduce other magnetic nuclei, chemically exchangeable groups, or hyperpolarized centres, will, however, almost certainly underpin beneficial developments.[153-158]

Few areas of research have exploded quite as dramatically as the development of both molecular and nanoparticle based image contrast and therapeutic delivery systems during the past decade. Applying the chemists’ toolkit and additionally integrating a non-invasive means of diagnosing and monitoring response to a treatment regime would, quite simply, herald a new age in clinical healthcare.

Acknowledgements

The authors acknowledge financial support from the Wellcome Trust (WT094114MA).

Biographies

Gemma-Louise Davies

Europe PMC Funders Author Manuscripts

Gemma-Louise Davies received her degree (2006) and PhD degree (2011) in Chemistry from Trinity College Dublin, Ireland. Her PhD involved the development of new silica and magnetic-luminescent silica nanostructured materials. She is currently working in the Department of Chemistry at the University of Oxford, UK with Dr Jason Davis. Her research interests encompass the preparation and characterisation of multifunctional nanomaterials as diagnostic and therapeutic tools in healthcare.

Iris Kramberger

Iris Kramberger received her Bachelor degree (2011) from University of Ljubljana, Slovenia and her Masters degree (2012) in Nanomaterials from Imperial College London, UK. She is currently studying towards her DPhil in Inorganic Chemistry from the University of Oxford, UK and is interested in the design and fabrication of ratiometric and stimuli-responsive inorganic and hydrogel based nanoparticle MRI agents.

Jason J. Davis

Jason Davis obtained a PhD in Chemistry from Oxford in 1998. After a Royal Society University Research Fellowship, he took up a lectureship at the University of Oxford before becoming a Reader in Chemistry. His research interests are broad and primarily focused on the use and development of state-of-the-art molecular, theranostic and medical imaging technologies as well as the design, analysis and manipulation of functional molecular interfaces.

Notes and references

1. Huang W-Y, Davis JJ. Dalton Trans. 2011; 40:6087. [PubMed: 21409202]
2. Pankhurst QA, Connolly J, Jones SK, Dobson J. J. Phys. D: Appl. Phys. 2003:R167.
3. Caravan P. Chem. Soc. Rev. 2006; 35:512. [PubMed: 16729145]
4. Corr SA, Byrne SJ, Tekoriute R, Meledandri CJ, Brougham DF, Lynch M, Kerskens C, O'Dwyer L, Gun'ko YK. J. Am. Chem. Soc. 2008; 130:4214. [PubMed: 18331033]

5. Davies G-L, Corr SA, Meledandri CJ, Briode L, Brougham DF, Gun'ko YK. ChemPhysChem. 2011; 12:772. [PubMed: 21387521]
6. Caravan P, Ellison JJ, McMurry TJ, Lauffer RB. Chem. Rev. 1999; 99:2293. [PubMed: 11749483]
7. Werner EJ, Datta A, Jocher CJ, Raymond KN. Angew. Chem., Int. Ed. 2008; 47:8568.
8. Lin C, Kadono T, Yoshizuka K, Furuichi T, Kawano T. Z. Naturforsch., C: J. Biosci. 2006; 61:74.
9. Oksendal AN, Hals P-A. J. Magn. Reson. Imaging. 1993; 3:157. [PubMed: 8428083]
10. Stasiuk GJ, Long NJ. Chem. Commun. 2013; 49:2732.
11. Comblin V, Gilsoul D, Hermann M, Humblet V, Jacques V, Mesbahi M, Sauvage C, Desreux JF. Coord. Chem. Rev. 1999; 185:451.
12. Aime S, Caravan P. J. Magn. Reson. Imaging. 2009; 30:1259. [PubMed: 19938038]
13. Villaraza AJL, Bumb A, Brechbiel MW. Chem. Rev. 2010; 110:2921. [PubMed: 20067234]
14. Solomon I. Phys. Rev. 1955; 99:559–565.
15. Bloembergen N, Purcell EM, Pound RV. Phys. Rev. 1948; 73:679.
16. Lowe MP, Parker D, Reany O, Aime S, Botta M, Castellano G, Gianolio E, Pagliarin R. J. Am. Chem. Soc. 2001; 123:7601. [PubMed: 11480981]
17. De Leon-Rodriguez LM, Lubag AJM, Malloy CR, Martinez GV, Gillies RJ, Sherry AD. Acc. Chem. Res. 2009; 42:948. [PubMed: 19265438]
18. Tu C, Osborne EA, Louie AY. Ann. Biomed. Eng. 2011; 39:1335. [PubMed: 21331662]
19. Major JL, Meade TJ. Acc. Chem. Res. 2009; 42:893. [PubMed: 19537782]
20. Logothetis NK. Nature. 2008; 453:869. [PubMed: 18548064]
21. Tu C, Louie AY. Chem. Commun. 2007:1331.
22. Aime S, Barge A, Botta M, Parker D, De Sousa AS. J. Am. Chem. Soc. 1997; 119:4767.
23. Aime S, Barge A, Bruce JI, Botta M, Howard JAK, Moloney JM, Parker D, de Sousa AS, Woods M. J. Am. Chem. Soc. 1999; 121:5762.
24. Zhang S, Wu K, Sherry AD. Angew. Chem., Int. Ed. 1999; 38:3192.
25. Kálmán FK, Woods M, Caravan P, Jurek P, Spiller M, Tircsó G, Király R, Brücher E, Sherry AD. Inorg. Chem. 2007; 46:5260. [PubMed: 17539632]
26. Aime S, Crich SG, Botta M, Giovenzana G, Palmisano G, Sisti M. Chem. Commun. 1999:1577.
27. Breckwoldt MO, Chen JW, Stangenberg L, Aikawa E, Rodriguez E, Qiu S, Moskowitz MA, Weissleder R. Proc. Natl. Acad. Sci. U. S. A. 2008; 105:18584. [PubMed: 19011099]
28. Moats RA, Fraser SE, Meade TJ. Angew. Chem., Int. Ed. Engl. 1997; 36:726.
29. Louie AY, Huber MM, Ahrens ET, Rothbacher U, Moats R, Jacobs RE, Fraser SE, Meade TJ. Nat. Biotechnol. 2000; 18:321. [PubMed: 10700150]
30. Duimstra JA, Femia FJ, Meade TJ. J. Am. Chem. Soc. 2005; 127:12847. [PubMed: 16159278]
31. Napolitano R, Pariani G, Fedeli F, Baranyai Z, Aswendt M, Aime S, Gianolio E. J. Med. Chem. 2013; 56:2466. [PubMed: 23469759]
32. Giardiello M, Lowe MP, Botta M. Chem. Commun. 2007:4044.
33. Caravan P, Cloutier NJ, Greenfield MT, McDermid SA, Dunham SU, Bulte JWM, Amedio JC, Looby RJ, Supkowski RM, Horrocks WD, McMurry TJ, Lauffer RB. J. Am. Chem. Soc. 2002; 124:3152. [PubMed: 11902904]
34. Nivorozhkin AL, Kolodziej AF, Caravan P, Greenfield MT, Lauffer RB, McMurry TJ. Angew. Chem., Int. Ed. 2001; 40:2903.
35. De León-Rodríguez LM, Ortiz A, Weiner AL, Zhang S, Kovacs Z, Kodadek T, Sherry AD. J. Am. Chem. Soc. 2002; 124:3514. [PubMed: 11929234]
36. Giardiello M, Botta M, Lowe M. J. Inclusion Phenom. Macrocyclic Chem. 2011; 71:435.
37. Noy D, Solomonov I, Sinkevich O, Arad T, Kjaer K, Sagi I. J. Am. Chem. Soc. 2008; 130:1376. [PubMed: 18179213]
38. Frederickson CJ, Koh J-Y, Bush AI. Nat. Rev. Neurosci. 2005; 6:449. [PubMed: 15891778]
39. Hanaoka K, Kikuchi K, Urano Y, Nagano T. J. Chem. Soc., Perkin Trans. 2. 2001:1840.
40. Hanaoka K, Kikuchi K, Urano Y, Narazaki M, Yokawa T, Sakamoto S, Yamaguchi K, Nagano T. Chem. Biol. 2002; 9:1027. [PubMed: 12323377]

41. Hifumi H, Tanimoto A, Citterio D, Komatsu H, Suzuki K. Analyst. 2007; 132:1153. [PubMed: 17955150]
42. Esqueda AC, López JA, Andreu-de-Riquer G, Alvarado-Monzón JC, Ratnakar J, Lubag AJM, Sherry AD, De León-Rodríguez LM. J. Am. Chem. Soc. 2009; 131:11387. [PubMed: 19630391]
43. De Leon-Rodriguez LM, Lubag AJM, Lopez JA, Andreu-de-Riquer G, Alvarado-Monzon JC, Sherry AD. MedChemComm. 2012; 3:480. [PubMed: 24013159]
44. Major JL, Parigi G, Luchinat C, Meade TJ. Proc. Natl. Acad. Sci. U. S. A. 2007; 104:13881. [PubMed: 17724345]
45. Major JL, Boiteau RM, Meade TJ. Inorg. Chem. 2008; 47:10788. [PubMed: 18928280]
46. Mishra A, Fousková P, Angelovski G, Balogh E, Mishra AK, Logothetis NK, Tóth É. Inorg. Chem. 2008; 47:1370. [PubMed: 18166011]
47. Angelovski G, Fouskova P, Mamedov I, Canals S, Toth E, Logothetis NK. ChemBioChem. 2008; 9:1729. [PubMed: 18604834]
48. Li W-H, Fraser SE, Meade TJ. J. Am. Chem. Soc. 1999; 121:1413.
49. Que EL, Chang CJ. J. Am. Chem. Soc. 2006; 128:15942. [PubMed: 17165700]
50. Que EL, Gianolio E, Baker SL, Wong AP, Aime S, Chang CJ. J. Am. Chem. Soc. 2009; 131:8527. [PubMed: 19489557]
51. Andrews M, Amoroso AJ, Harding LP, Pope SJA. Dalton Trans. 2010; 39:3407. [PubMed: 20379534]
52. Que EL, New EJ, Chang CJ. Chem. Sci. 2012; 3:1829. [PubMed: 25431649]
53. Li W-S, Luo J, Chen Z-N. Dalton Trans. 2011; 40:484. [PubMed: 21113542]
54. Kasala D, Lin T-S, Chen C-Y, Liu G-C, Kao C-L, Cheng T-L, Wang Y-M. Dalton Trans. 2011; 40:5018. [PubMed: 21451883]
55. Mishra A, Logothetis NK, Parker D. Chem.-Eur. J. 2011; 17:1529. [PubMed: 21268155]
56. Kubíček V, Vitha T, Kotek J, Hermann P, Vander Elst L, Muller RN, Lukeš I, Peters JA. Contrast Media Mol. Imaging. 2010; 5:294. [PubMed: 20973114]
57. Lubag AJM, De Leon-Rodriguez LM, Burgess SC, Sherry AD. Proc. Natl. Acad. Sci. U. S. A. 2011; 108:18400. [PubMed: 22025712]
58. Aime S, Botta M, Fasano M, Terreno E. Spectrochim. Acta, Part A. 1993; 49:1315.
59. Livramento JB, Sour A, Borel A, Merbach AE, Tóth É. Chem.-Eur. J. 2006; 12:989. [PubMed: 16311990]
60. Parac-Vogt TN, Vander Elst L, Kimpe K, Laurent S, Burtéa C, Chen F, Van Deun R, Ni Y, Muller RN, Binnemans K. Contrast Media Mol. Imaging. 2006; 1:267. [PubMed: 17191767]
61. Paris J, Gameiro C, Humblet V, Mohapatra PK, Jacques V, Desreux JF. Inorg. Chem. 2006; 45:5092. [PubMed: 16780331]
62. Muller RN, Radüchel B, Laurent S, Platzek J, Piérart C, Mareski P, Vander Elst L. Eur. J. Inorg. Chem. 1999:1949.
63. Gillies RJ, Raghunand N, Garcia-Martin ML, Gatenby RA. IEEE Eng. Med. Biol. 2004; 23:57.
64. Wike-Hooley JL, Haveman J, Reinhold HS. Radiother. Oncol. 1984; 2:343. [PubMed: 6097949]
65. Rockwell S, Dobrucki IT, Kim EY, Marrison ST, Vu V. T. h. u. c. Curr. Mol. Med. 2009; 9:442. [PubMed: 19519402]
66. Hall J, Haner R, Aime S, Botta M, Faulkner S, Parker D, de Sousa AS. New J. Chem. 1998; 22:627.
67. Garcia-Martin ML, Martinez GV, Raghunand N, Sherry AD, Zhang S, Gillies RJ. Magn. Res. Med. 2006; 55:309.
68. Aime S, Fedeli F, Sanino A, Terreno E. J. Am. Chem. Soc. 2006; 128:11326. [PubMed: 16939235]
69. Gianolio E, Maciocco L, Imperio D, Giovenzana GB, Simonelli F, Abbas K, Bisi G, Aime S. Chem. Commun. 2011; 47:1539.
70. Frullano L, Catana C, Benner T, Sherry AD, Caravan P. Angew. Chem., Int. Ed. 2010; 49:2382.
71. Hyodo F, Chuang K-H, Goloshevsky AG, Sulima A, Griffiths GLL, Mitchell JBB, Koretsky AP, Krishna MC. J. Cereb. Blood Flow Metab. 2008; 28:1165. [PubMed: 18270519]
72. Klaidman LK, Leung AC, Adams JD. Anal. Biochem. 1995; 228:312. [PubMed: 8572312]

73. Hyodo F, Soule BP, Matsumoto K-I, Matusmoto S, Cook JA, Hyodo E, Sowers AL, Krishna MC, Mitchell JB. J. Pharm. Pharmacol. 2008; 60:1049. [PubMed: 18644197]
74. Tu C, Nagao R, Louie AY. Angew. Chem., Int. Ed. 2009; 48:6547.
75. Tu C, Osborne EA, Louie AY. Tetrahedron. 2009; 65:1241. [PubMed: 20126289]
76. Raghunand N, Jagadish B, Trouard TP, Galons J-P, Gillies RJ, Mash EA. Magn. Res. Med. 2006; 55:1272.
77. Burai L, Scopelliti R, Toth E. Chem. Commun. 2002:2366.
78. Aime S, Botta M, Gianolio E, Terreno E. Angew. Chem., Int. Ed. 2000; 39:747.
79. Hernandez G, Bryant RG. Bioconjugate Chem. 1991; 2:394.
80. Bryant LH, Hodges MW, Bryant RG. Inorg. Chem. 1999; 38:1002. [PubMed: 11670874]
81. Burai L, Tóth É, Moreau G, Sour A, Scopelliti R, Merbach AE. Chem.-Eur. J. 2003; 9:1394. [PubMed: 12645029]
82. de Wet JR, Wood KV, DeLuca M, Helinski DR, Subramani S. Mol. Cell. Biol. 1987; 7:725. [PubMed: 3821727]
83. Cheung ENM, Alvares RDA, Oakden W, Chaudhary R, Hill ML, Pichaandi J, Mo GCH, Yip C, Macdonald PM, Stanisz GJ, van Veggel FCJM, Prosser RS. Chem. Mater. 2010; 22:4728.
84. Platas-Iglesias C, Vander Elst L, Zhou WZ, Muller RN, Geraldes C, Maschmeyer T, Peters JA. Chem.-Eur. J. 2002; 8:5121. [PubMed: 12613030]
85. Ananta JS, Godin B, Sethi R, Moriggi L, Liu X, Serda RE, Krishnamurthy R, Muthupillai R, Bolskar RD, Helm L, Ferrari M, Wilson LJ, Decuzzi P. Nat. Nanotechnol. 2010; 5:815. [PubMed: 20972435]
86. Hartman KB, Laus S, Bolskar RD, Muthupillai R, Helm L, Toth E, Merbach AE, Wilson LJ. Nano Lett. 2008; 8:415. [PubMed: 18215084]
87. Evanics F, Diamente PR, van Veggel F, Stanisz GJ, Prosser RS. Chem. Mater. 2006; 18:2499.
88. Hou Y, Qiao R, Fang F, Wang X, Dong C, Liu K, Liu C, Liu Z, Lei H, Wang F, Gao M. ACS Nano. 2013; 7:330. [PubMed: 23199030]
89. Li Y, Beija M, Laurent S, vander Elst L, Muller RN, Duong HTT, Lowe AB, Davis TP, Boyer C. Macromolecules. 2012; 45:4196.
90. Laus S, Sour A, Ruloff R, Toth E, Merbach AE. Chem.-Eur. J. 2005; 11:3064. [PubMed: 15776490]
91. Fossheim SL, Fahlvik AK, Klaveness J, Muller RN. Magn. Reson. Imaging. 1999; 17:83. [PubMed: 9888401]
92. Mi P, Cabral H, Kokuryo D, Rafi M, Terada Y, Aoki I, Saga T, Takehiko I, Nishiyama N, Kataoka K. Biomaterials. 2013; 34:492. [PubMed: 23059004]
93. Caravan P, Parigi G, Chasse JM, Cloutier NJ, Ellison JJ, Lauffer RB, Luchinat C, McDermid SA, Spiller M, McMurry TJ. Inorg. Chem. 2007; 46:6632. [PubMed: 17625839]
94. Carniato F, Tei L, Dastru W, Marchese L, Botta M. Chem. Commun. 2009:1246.
95. Marradi M, Alcantara D, de la Fuente JM, Garcia-Martin ML, Cerdan S, Penades S. Chem. Commun. 2009:3922.
96. Peters JA, Djanashvili K. Eur. J. Inorg. Chem. 2012:1961.
97. Botta M, Tei L. Eur. J. Inorg. Chem. 2012:1945.
98. Bottrill M, Kwok L, Long NJ. Chem. Soc. Rev. 2006; 35:557. [PubMed: 16729149]
99. Lowe MP. Aust. J. Chem. 2002; 55:551–556.
100. Lauffer RB, Brady TJ. Magn. Reson. Imaging. 1985; 3:11. [PubMed: 3923289]
101. Kielar F, Tei L, Terreno E, Botta M. J. Am. Chem. Soc. 2010; 132:7836. [PubMed: 20481537]
102. Nicolle GM, Toth E, Eisenwiener KP, Macke HR, Merbach AE. J. Biol. Inorg. Chem. 2002; 7:757. [PubMed: 12203012]
103. Tang J, Sheng Y, Hu H, Shen Y. Prog. Polym. Sci. 2013; 38:462.
104. Zong Y, Guo J, Ke T, Mohs AM, Parker DL, Lu Z-R. J. Controlled Release. 2006; 112:350.
105. Peng H, Blakey I, Dargaville B, Rasoul F, Rose S, Whittaker AK. Biomacromolecules. 2009; 10:374. [PubMed: 19128056]

106. Xu Q, Zhu L, Yu M, Feng F, An L, Xing C, Wang S. Polymer. 2010; 51:1336.
107. Okada S, Mizukami S, Kikuchi K. Bioorg. Med. Chem. 2012; 20:769. [PubMed: 22206870]
108. Turner JL, Pan D, Plummer R, Chen Z, Whittaker AK, Wooley KL. Adv. Funct. Mater. 2005; 15:1248.
109. Kojima C, Turkbey B, Ogawa M, Bernardo M, Regino CAS, Bryant LH Jr, Choyke PL, Kono K, Kobayashi H. Nanomed.: Nanotechnol., Biol. Med. 2011; 7:1001.
110. He C, Wu X, Kong J, liu T, Zhang X, Duan C. Chem. Commun. 2012; 48:9290.
111. Huang W-Y, Davies G-L, Davis JJ. Chem. Commun. 2013; 49:60.
112. Okada S, Mizukami S, Kikuchi K. ChemBioChem. 2010; 11:785. [PubMed: 20209557]
113. Tilcock C, Ahkong QF, Koenig SH, Brown RD, Davis M, Kabalka G. Magn. Res. Med. 1992; 27:44.
114. Alhaique F, Bertini I, Fragai M, Carafa M, Luchinat C, Parigi G. Inorg. Chim. Acta. 2002; 331:151.
115. Storrs RW, Tropper FD, Li HY, Song CK, Kuniyoshi JK, Sipkins DA, Li KCP, Bednarski MD. J. Am. Chem. Soc. 1995; 117:7301.
116. Pütz B, Barsky D, Schulten K. J. Liposome Res. 1994; 4:771.
117. Davis JJ, Huang W-Y, Davies G-L. J. Mater. Chem. 2012; 22:22848. [PubMed: 26052183]
118. Taylor KML, Kim JS, Rieter WJ, An H, Lin W, Lin W. J. Am. Chem. Soc. 2008; 130:2154. [PubMed: 18217764]
119. Sethi R, Ananta JS, Karmonik C, Zhong M, Fung SH, Liu X, Li K, Ferrari M, Wilson LJ, Decuzzi P. Contrast Media Mol. Imaging. 2012; 7:501. [PubMed: 22991316]
120. Carniato F, Tei L, Cossi M, Marchese L, Botta M. Chem.-Eur. J. 2010; 16:10727. [PubMed: 20669190]
121. Dhingra Verma K, Mishra A, Engelmann J, Beyerlein M, Maier ME, Logothetis NK. ChemPlusChem. 2012; 77:758.
122. Datta A, Hooker JM, Botta M, Francis MB, Aime S, Raymond KN. J. Am. Chem. Soc. 2008; 130:2546. [PubMed: 18247608]
123. Hossann M, Wang T, Syunyaeva Z, Wiggenhorn M, Zengerle A, Issels RD, Reiser M, Lindner LH, Peller M. J. Controlled Release. 2013; 166:22.
124. Lin C-W, Tseng SJ, Kempson IM, Yang S-C, Hong T-M, Yang P-C. Biomaterials. 2013; 34:4387. [PubMed: 23478033]
125. Vibhute SM, Engelmann J, Verbic T, Maier ME, Logothetis NK, Angelovski G. Org. Biomol. Chem. 2013; 11:1294. [PubMed: 23223612]
126. Schopf E, Sankaranarayanan J, Chan M, Mattrey R, Almutairi A. Mol. Pharmaceutics. 2012; 9:1911.
127. Schmaljohann D. Adv. Drug Delivery Rev. 2006; 58:1655.
128. Gianolio E, Napolitano R, Fedeli F, Arena F, Aime S. Chem. Commun. 2009:6044.
129. Woods M, Kiefer GE, Bott S, Castillo-Muzquiz A, Eshelbrenner C, Michaudet L, McMillan K, Mudigunda SDK, Ogrin D, Tircsó G, Zhang S, Zhao P, Sherry AD. J. Am. Chem. Soc. 2004; 126:9248. [PubMed: 15281814]
130. Almeida H, Amaral MH, Lobão P. J. Appl. Pharm. Sci. 2012; 2:1.
131. Aime S, Botta M, Crich SG, Giovenzana G, Palmisano G, Sisti M. Chem. Commun. 1999:1577.
132. Aime S, Fedeli F, Sanino A, Terreno E. J. Am. Chem. Soc. 2006; 128:11326. [PubMed: 16939235]
133. Borel A, Helm L, Merbach AE. Chem.-Eur. J. 2001; 7:600. [PubMed: 11261657]
134. Ali MM, Woods M, Caravan P, Opina ACL, Spiller M, Fettinger JC, Sherry AD. Chem.-Eur. J. 2008; 14:7250. [PubMed: 18601236]
135. Gianolio E, Porto S, Napolitano R, Baroni S, Giovenzana GB, Aime S. Inorg. Chem. 2012; 51:7210. [PubMed: 22716284]
136. Martinelli J, Fekete M, Tei L, Botta M. Chem. Commun. 2011; 47:3144.
137. Liang G, Ronald J, Chen Y, Ye D, Pandit P, Ma ML, Rutt B, Rao J. Angew. Chem., Int. Ed. 2011; 50:6283.

138. Cao C-Y, Shen Y-Y, Wang J-D, Li L, Liang G-L. Sci. Rep. 2013; 3:1.
139. Galiana G, Branca RT, Jenista ER, Warren SW. Science. 2008; 322:421. [PubMed: 18927389]
140. Grüll H, Langereis S. J. Controlled Release. 2012; 161:317.
141. Terreno E, Sanino A, Carrera C, Castelli DD, Giovenzana GB, Lombardi A, Mazzon R, Milone L, Visigalli M, Aime S. J. Inorg. Biochem. 2008; 102:1112. [PubMed: 18329102]
142. Strijkers GJ, Mulder WJM, van Heeswijk RB, Frederik PM, Bomans P, Magusin PCMM, Nicolay K. Magn. Reson. Mater. Phys., Biol. Med. 2005; 18:186.
143. de Smet M, Langereis S, van den Bosch S, Grüll H. J. Controlled Release. 2010; 143:120.
144. Tagami T, Foltz WD, Ernsting MJ, Lee CM, Tannock IF, May JP, Li S-D. Biomaterials. 2011; 32:6570. [PubMed: 21641639]
145. Shuhendler AJ, Staruch R, Oakden W, Gordijo CR, Rauth AM, Stanisz GJ, Chopra R, Wu XY. J. Controlled Release. 2012; 157:478.
146. Lehner R, Wang X, Wolf M, Hunziker P. J. Controlled Release. 2012; 161:307.
147. Vandsburger MH, Radoul M, Cohen B, Neeman M. NMR Biomed. 2012:1. [PubMed: 21538636]
148. Zhang Z, Greenfield MT, Spiller M, McMurry TJ, Lauffer RB, Caravan P. Angew. Chem., Int. Ed. 2005; 44:6766.
149. Xu W, Lu Y. Chem. Commun. 2011; 47:4998.
150. Swanson SD, Kukowska-Latallo JF, Patri AK, Chen C, Ge S, Cao Z, Kotlyar A, East AT, Baker JR. Int. J. Nanomed. 2008; 3:201.
151. Caravan P, Greenwood JM, Welch JT, Franklin SJ. Chem. Commun. 2003:2574.
152. Catanzaro V, Gringeri CV, Menchise V, Padovan S, Boffa C, Dastrù W, Chaabane L, Digilio G, Aime S. Angew. Chem., Int. Ed. 2013; 52:3926.
153. Villaraza AJL, Bumb A, Brechbiel MW. Chem. Rev. 2010; 110:2921. [PubMed: 20067234]
154. Viswanathan S, Kovacs Z, Green KN, Ratnakar SJ, Sherry AD. Chem. Rev. 2010; 110:2960. [PubMed: 20397688]
155. Ward KM, Aletras AH, Balaban RS. J. Magn. Reson. 2000; 143:79. [PubMed: 10698648]
156. Wolff SD, Balaban RS. Magn. Res. Med. 1989; 10:135.
157. Ward KM, Balaban RS. Magn. Res. Med. 2000; 44:799.
158. Glunde K, Artemov D, Penet M-F, Jacobs MA, Bhujwalla ZM. Chem. Rev. 2010; 110:3043. [PubMed: 20384323]
159. Løkling K-E, Skurtveit R, Dyrstad K, Klaveness J, Fossheim SL. Int. J. Pharm. 2004; 274:75. [PubMed: 15072784]
160. Vibhute SM, Engelmann J, Verbic T, Maier ME, Logothetis NK, Angelovski G. Org. Biomol. Chem. 2013; 11:1294. [PubMed: 23223612]
161. Toth E, Bolskar RD, Borel A, Gonzalez G, Helm L, Merbach AE, Sitharaman B, Wilson LJ. J. Am. Chem. Soc. 2005; 127:799. [PubMed: 15643906]
162. Kim T, Cho E-J, Chae Y, Kim M, Oh A, Jin J, Lee E-S, Baik H, Haam S, Suh J-S, Huh Y-M, Lee K. Angew. Chem., Int. Ed. 2011; 50:10589.
163. Chen Y, Yin Q, Ji X, Zhang S, Chen H, Zheng Y, Sun Y, Qu H, Wang Z, Li Y, Wang X, Zhang K, Zhang L, Shi J. Biomaterials. 2012; 33:7126. [PubMed: 22789722]
164. Szabo I, Crich SG, Alberti D, Kalman FK, Aime S. Chem. Commun. 2012; 48:2436.
165. Li Y, Qian Y, Liu T, Zhang G, Liu S. Biomacromolecules. 2012; 13:3877. [PubMed: 23013152]

Europe PMC Funders Author Manuscripts

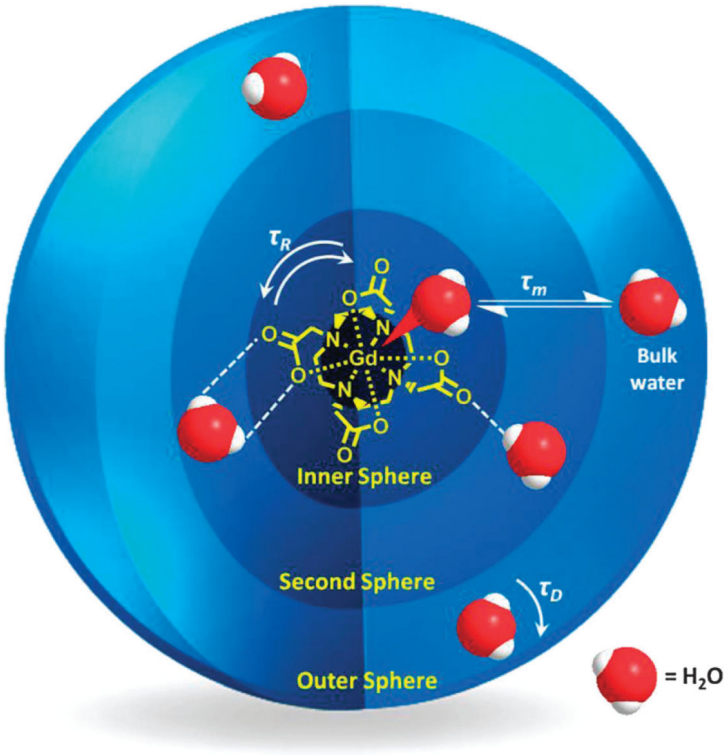

Fig. 1.

Schematic representation of inner, second and outer sphere water interaction with a typical T_1 contrast agent, a Gd–DOTA chelate.

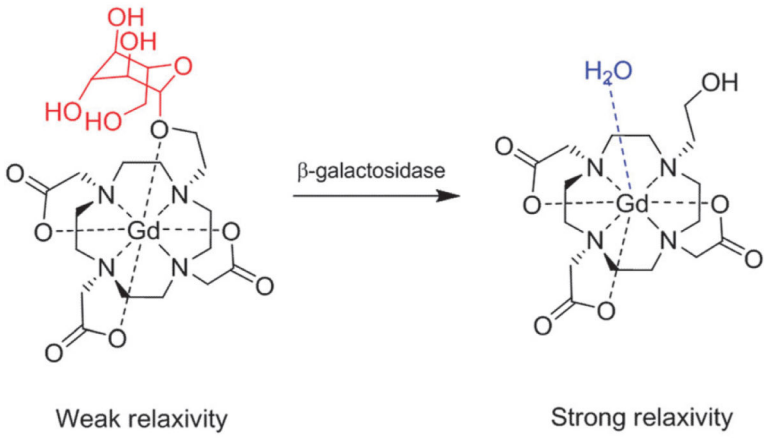

Fig. 2.

Schematic representation of Egad MRI contrast agent; galactopyranose groups (red) are removed *via* β-galactosidase cleavage, resulting in an irreversible transition from a weak to a strong relaxivity state, reproduced with permission from ref. 28. Copyright 1997 Wiley-VCH Verlag GmbH & Co. KGaA.

Europe PMC Funders Author Manuscripts

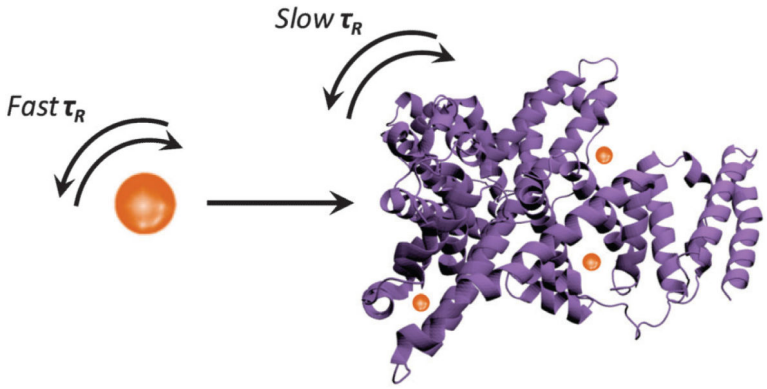

Fig. 3.

Illustration of the generic association between a Gd^{3+} chelate (brown sphere) and a protein target (purple) resulting in lengthened τ_R and improved MRI contrast.

Europe PMC Funders Author Manuscripts

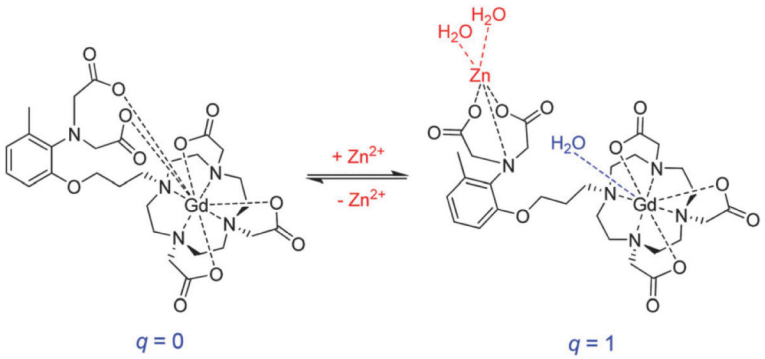

Fig. 4.

A proposed mechanism of MRI relaxivity modulation based on hydration (*q*) alterations due to pendant acetate coordination in the presence of Zn^{2+} ions, adapted with permission from ref. 45. Copyright 2008 American Chemical Society.

Europe PMC Funders Author Manuscripts

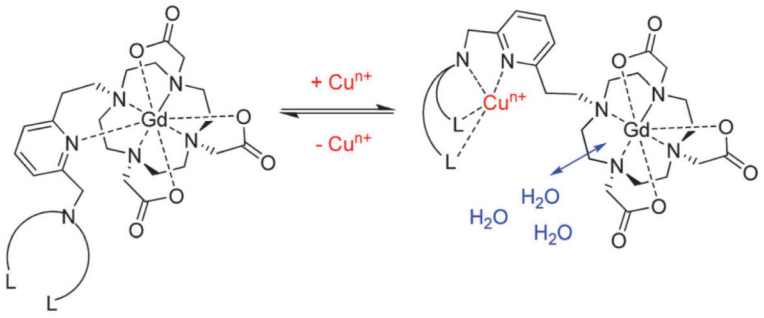

Fig. 5.

Representation of MRI contrast agent species with $Cu^{+/2+}$ selectivity, where L is a ligand, such as a thioether-based donor, n = 1, 2; adapted with permission from ref. 50. Copyright 2009 American Chemical Society.

Europe PMC Funders Author Manuscripts

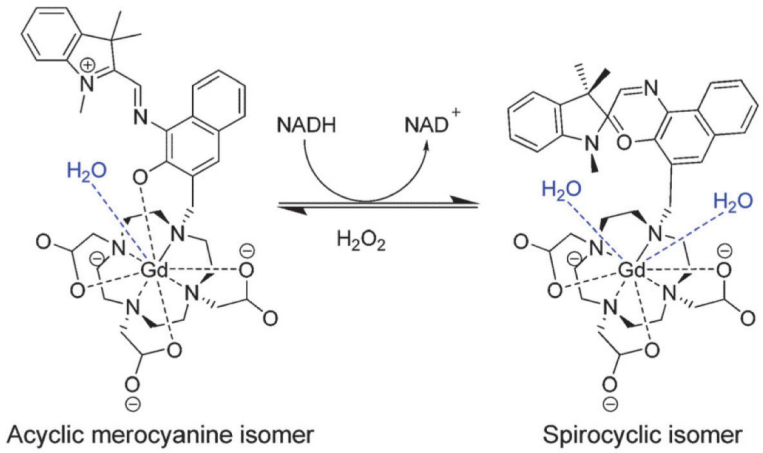

Fig. 6.

Redox-sensitive structural isomerisation of spiropyran–merocyaninetethered GdDOTA, adapted with permission from ref. 74. Copyright 2009 Wiley-VCH Verlag GmbH & Co. KGaA.

Europe PMC Funders Author Manuscripts

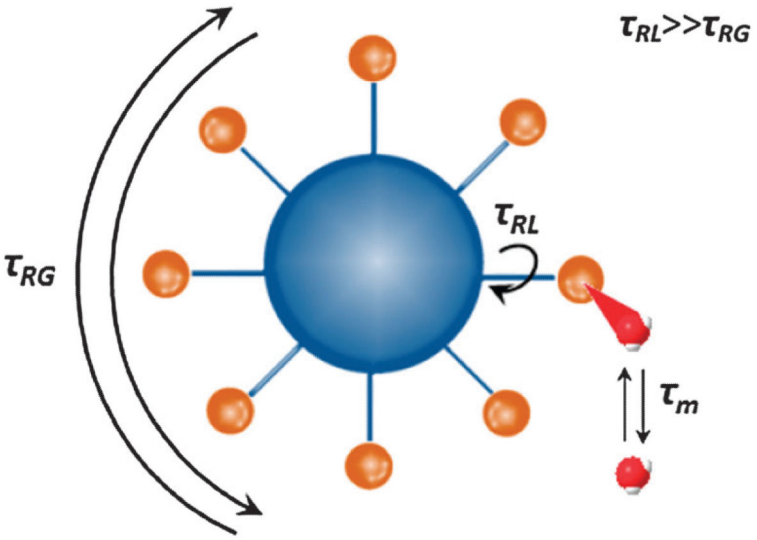

Fig. 7.

The relaxivity of a nanoparticulate MRI probe (blue sphere) with conjugated Gd^{3+}-complexes (brown spheres) is determined by the local rotational time of the complex around the linker (τ_{RL}), the global rotational motion (τ_{RG}), and the coordinated water exchange rate ($k_{ex} = 1/\tau_m$). Adapted with permission from ref. 97. Copyright 2012 Wiley-VCH Verlag GmbH & Co. KGaA.

Europe PMC Funders Author Manuscripts

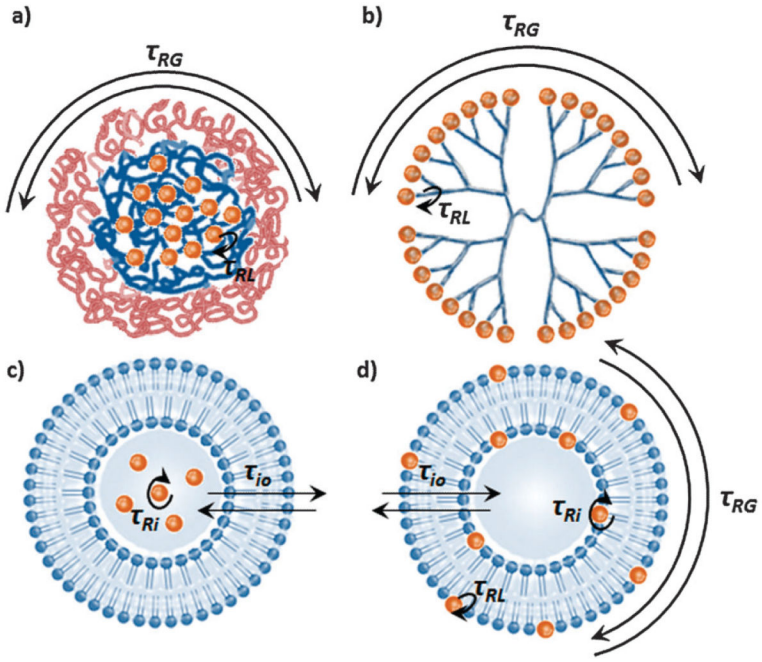

Fig. 8.

Schematic representation of local and global mobility processes relevant to Gd^{3+}-chelates (brown spheres) in (a) cross-linked polymeric nanoparticles, (b) dendrites, (c) enosomes, and (d) memsomes with τ_{RG} and τ_{RL} representing global and local rotational correlation times, respectively. Paramagnetic chelates are covalently bound in (a) and (b); for the paramagnetic chelates encapsulated (in (c) and (d)) in the membrane or aqueous phase of a liposome, τ_{io} denotes water exchange rate between the interior and exterior and τ_{Ri} the rotational correlation time of the internalised complex.

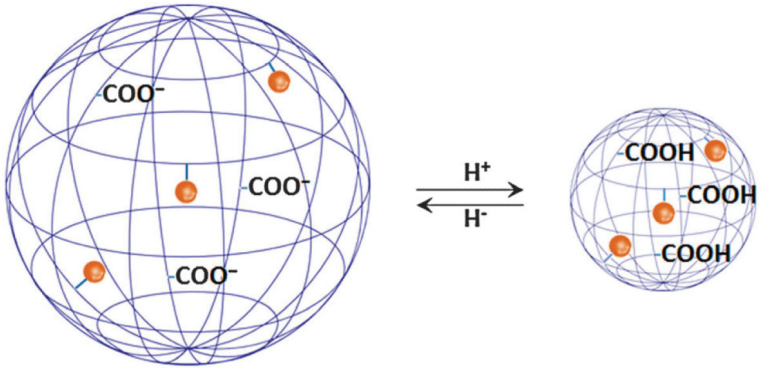

Fig. 9.

The carboxylic groups of anionic polymeric nanoparticulates are progressively deionised when exposed to an acidic environment resulting in polymer shrinking, restricted side chain mobility, and significantly increasing relaxivity.[107] The blue net represents the polymer and brown spheres the Gd^{3+}-chelate groups covalently conjugated to polymer side chains. Picture adapted with permission from ref. 130.

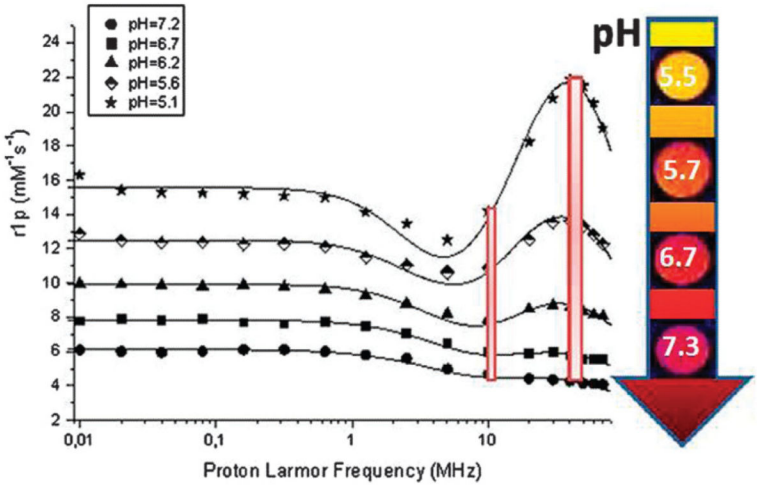

Fig. 10.

NMRD profile showing the pH tuned ^{1}H longitudinal relaxivity of LUV loaded with a Gd^{3+}–DO3A derivative (1 mM [Gd]) as a function of applied magnetic field. The colour scale bar in the arrow denotes the signal intensities of T_1-weighted images, and the two red bars represent ^{1}H relaxivities at two different magnetic fields (8.5 MHz and 40 MHz). Adapted with permission from ref. 135. Copyright 2012 American Chemical Society.

Europe PMC Funders Author Manuscripts

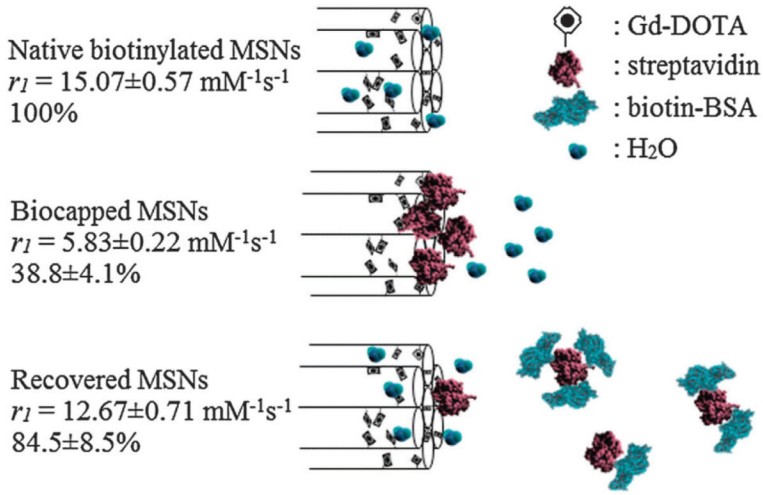

Fig. 11.

Schematic summary of the protein gating of MSNs. Externally biotinylated Gd–DOTA MSNs enjoy good water accessibility and a high relaxivity that can be reversibly capped by the steric bulk of bound streptavidin. In the presence of low μM of biotinylated BSA, the gating protein is competed off the particle surface and relaxivity recovers. Adapted from ref. 111 with permission from The Royal Society of Chemistry.

Table 1

Summary of relaxivity responses to various environmental stimuli of molecular, macromolecular, polymeric and particulate MRI CAs

Responsive MRI probe	Stimulus	Mechanistic change	r_1 switch [mM^{-1} s^{-1}]	Percentage change	Ref.
Molecular MRI CAs					
4,7,10-Tri(acetic acid)-1-(2-β-galactopyranosylethoxy)-1,4,7,10-tetraazacyclododecane gadolinium (EGad)	β-Galactosidase	q	Not reported	20% decrease	28
(l-(2-(β-Glalactopyranosyloxy)propyl)-4,5,10-tris(carboxymethyl-1,4,7,10-tetra-azacyclododecane))gadolinium (EGadMe)	β-Galactosidase	q	0.90–2.72 s^{-1} [a] at 500 MHz	200% increase	29
Gd–DO3A bearing a pendant β-glucuronic acid moiety connected by a self-immolative linker	β-Glucuronidase	q	4.75–3.90 at 60 MHz	20% decrease	30
Gd–DO3A appended with acetoxymethyl esters	Porcine liver esterase	q	5.7–10.8 at 20 MHz	89% increase	32
Bis-5-hydroxytryptamide-diethylenetriamine-pentatacetate gadolinium (MPO–Gd)	Myeloperoxidase (MPO)	τ_R	Not reported	Not reported	27
Gd–DTPA with phosphonate side chain (MS-325)	Human serum albumin (HSA)	τ_R	5.6–50.8 at 20 MHz	800% increase at 20 MHz	33
			5.0–25.0 at 64 MHz	400% increase at 64 MHz	
Gd–DTPA appended with lysine residues	Thrombin-activatable fibrinolysis inhibitor (TAFI)	τ_R	12.5–25.2 at 20 MHz	100% increase	34
Gd–DOTA with pendant diphenylphosphinamide groups	Human serum albumin (HSA)	τ_R	7.3–16.0 at 20 MHz	119% increase	36
Gd–DO3A–glutamate	Glutamic acid decarboxylase (GAD)	q, τ_R	8.0–11.5 at 20 MHz	44% increase	31
Peptide-labelled GdDO3A (Gd^{3+}–G80BP)	Ga180 protein	τ_R	8.3–44.8 at 20 MHz	440% increase	35
Gd–DTPA bisamide	Zn^{2+}	q	6.06–3.98 at 300 MHz	34% decrease	39
Gd–DTPA bisamide	Zn^{2+}	q	4.8–3.5 at 300 MHz	27% decrease	40
Gd–DTPA-appended β-diketone (KMR–Mg)	Mg^{2+} (also Ca^{2+})	q	4.98–3.95 at 20 MHz	21% decrease	41
Gd–DOTA appended with *N*,*N*-bis(2-pyridyl-methyl) ethylene diamine (bisBPEN) diamide	Zn^{2+}, Cu^{2+}	k_{ex}	5.0–6.0 at 23 MHz	20% increase	42
Gd–DOTA appended with two bis-(3-pyrazolyl) units	Zn^{2+}, Cu^{2+}	k_{ex}	4.2–6.9 at 23 MHz	64% increase	43
Gd–diaminoacetate with 3 methylenes (Gd–daa3)	Zn^{2+}	q	2.3–5.1 at 60 MHz	121% increase	44, 45
Gd[l,2-bis[{[({l-[l,4,7-tris(carboxymethyl)-1,4,7,10-tetra-azacyclododecane-10-yl]eth-2-yl}amino)carbonyl]methyl}-(carboxymethyl)amino]ethane]	Ca^{2+}	q	5.4–7.1 at 500 MHz	32% increase	46
Ethylene glycol tetraacetic acid (EGTA) linked to 2 Gd–DO3A chelates	Ca^{2+}	q	3.44–6.29 at 500 MHz	83% increase	47
DOPTA–Gd	Ca^{2+}	q	3.26–5.76 at 500 MHz	80% increase	48
Gd–DO3A chelate with pyro-EGTA moiety	Ca^{2+}, Zn^{2+}	q	3.8–6.6 at 60 MHz	73% increase	55
Gd–DO3A with a pendant iminodiacetate	Cu^{2+}	q	3.76–5.29 at 400 MHz	41% increase	49

Responsive MRI probe	Stimulus	Mechanistic change	r_1 switch [mM^{-1} s^{-1}]	Percentage change	Ref.
Gd–DO3A with tethered thioether groups	Cu^{2+}	*q*	1.5–6.9 at 20 MHz	360% increase	50
Octaarginine-conjugated Gd–DO3A with tethered thioether groups	Cu^{+}	*q*	3.9–12.5 at 60 MHz	220% increase	52
Gd–DO3A with appended 8-amidequinoline (Gd-QDOTAMA)	Cu^{2+}	*q*	4.27–7.29 at 400 MHz	71% increase	53
Tryptophan-appended Gd–TTDA [Gd(Try-TTDA)(H_2O)]2^{-}	Cu^{2+}	*q*	4.22–7.42 at 20 MHz	76% increase	54
Di-metallic-DO3A with piperazine bridge	Hg^{2+}	*q*	8.3–10.3 at 30 MHz	24% increase	51
GdDOTA–diBPEN	Zn^{2+}	τ_R	5.0–17.5 at 23 MHz	250% increase	57
Gd(phen)HDO3A chelate	Fe^{2+}	τ_R	3.7–12.2 at 20 MHz	230% increase	11
$[Gd_2bpy(DTTA)_2(H_2O)_4]^{2-}$	Fe^{2+}	τ_R	12.44–20.17 at 20 MHz	62% increase	59
Terpyridine–Gd^{3+} chelate	pH	*q*	12.8–2.0 at 20 MHz	84%	66
[Gd(DOTA tetrakis(methylamide))]$^{3+}$	pH	τ_m	2.5–5.7 at 20 MHz	128%	22, 23
Dinitrospiropyran–GdDO3A	NADH	*q*	2.51–1.86 at 60 MHz	26% decrease	74, 75
Spiropyran–GdDO3A	NADH	*q*	5.58–8.60 at 60 MHz	54% increase	74
Spiropyran–GdDO3A	Light	*q*	3.72–2.93 at 60 MHz	21% decrease	75
Macromolecular, polymeric and particulate MRI CAs					
G5-PAMAM dendrimer with Gd-complexes bearing phosphonate pendant arms	pH	τ_R, τ_m	10.8–24.0 at 20 MHz	122%	134
Large unilamellar vesicles (POPC/DPPC) loaded with the an amphiphilic GdDO3A derivative	pH	τ_R, τ_m	4.5–13.5 at 43 MHz	200%	135
Sulfonamide arm containing Gd-chelate hosted by poly-β-cyclodextrin	pH	*q*	8–16 at 43 MHz	100%	128
Diacylphosphatidylethanolamine/ dipalmitoylglycerosuccinate based enosome loaded with a GdDTPA-derivative	pH	τ_{io}	2.3–0.7 at 20 MHz	228%	159
Poly-L-ornithine	pH	τ_R, τ_m	23.0–32.0 at 20 MHz	39%	131
Methacrylic acid based polymer cross-linked by *N*,*N*′-methylenebisacrylamide	pH	Swelling (τ_R)	Non-cross-linked polymer: 6.7–12.1 Cross-linked polymer: 13.6–28.0 at 20 MHz	106%	107
n-Octylamine modified poly(SM-EVE) polymer loaded with aminoethyl-modified GdDO3A	pH	Electrostatic repulsion (high pH), hydrophobic interaction (low pH) (τ_R)	8.0–9.0 at 20 MHz	12%	112
Avidin conjugated to GdDOTA derivative with a phosphonate pendant arm	pH	τ_R, *q*	10.4–12.6 at 128 MHz	21%	160

Responsive MRI probe	Stimulus	Mechanistic change	r_1 switch [mM^{-1} s^{-1}]	Percentage change	Ref.
Ketal-based polymer with a GdDTPA derivative	pH	Polymer degradation (τ_R)	8.2–3.8 at 64 MHz	115%	126
Gadonanotubes	pH	Gd^{3+} loss	40.0–133.0 at 64 MHz	233%	86
Gadofullerenes	pH	Aggregation (τ_R)	10.4–38.5 at 30–60 MHz	270%	161
Manganese oxide nanoparticles	pH	Release of Mn^{2+} ions	8.8–27.7 at 64 MHz	215%	162
Manganese oxide functionalised mesoporous silica nanoparticle	pH	Dissolution	0.8–8.8 at 128 MHz	1015%	163
GdDOTA doped mesoporous silica nanoparticles capped by streptavidin	Biotinylated BSA	τ_m	5.8–12.7 at 300 MHz	219% increase	111
Hexanuclear gadolinium organic octahedron	Glucosamine	k_{ex}, q	388.5–62.1 at 400 MHz	526% decrease	110
Manganese loaded apoferritin	Melanin	Reduction, dissolution (τ_R)	0.3–6.0 at 300 MHz	1900% increase	164
DNA aptamer conjugated to streptavidin and GdDOTA	Adenosine	Release of Gd-DNA strand (τ_R)	12.2–9.2 at 60 MHz	33% decrease	149
Liposome with incorporated amphiphilic GdDOTA covalently linked to a peptide sequence	Metalloproteinase-2	τ_R	8.9–7.5 at 60 MHz	16% decrease	152
GdDOTA covalently coupled to a chemically modified peptide sequence bearing a cyano and 1,2-aminothiol group	Furin	Reduction, self-assembly into nanoparticles (τ_R)	6.0–13.2 at 64 MHz	220% increase	137
Perthiolated β-cyclodextrin-based nanocapsules	Reductive/hypoxic environment	Reduction, degradation (τ_R)	15.2–8.2 at 70 MHz	46% decrease	136
P(NIPAM)-*co*-P(AM) hydrogel nanoparticles cross-linked by a GdDTPA-derivative and loaded into solid lipid nanoparticles	Temperature	k_{ex}, τ_{io}, τ_R	12.4–8.6 at 300 MHz	44% decrease	145
POEGMA-*b*-P(NIPAM-*co*-NBA-*co*-Gd) diblock copolymer	Temperature	k_{ex}	6.5–12.1 at 300 MHz	86% increase	165
Liposomes loaded with Gd-complexes	Temperature	τ_{io}	1828–394 ms[b] at 300 MHz	364% decrease	143

[a] Relaxation rate provided in s^{-1}.

[b] Relaxation time provided in ms.